

Probing Electroweak Baryogenesis induced by extra bottom Yukawa coupling in $bg \rightarrow bA \rightarrow bt\bar{t}$ signature

Tanmoy Modak^{1,2} and Eibun Senaha^{3,4}

¹*Department of Physics, Osaka University, Toyonaka, Osaka 560-0043, Japan*

²*Department of Physics, National Taiwan University, Taipei 10617, Taiwan*

³*Theoretical Particle Physics and Cosmology Research Group,*

Advanced Institute of Materials Science,

Ton Duc Thang University, Ho Chi Minh City, Vietnam

⁴*Faculty of Applied Sciences, Ton Duc Thang University, Ho Chi Minh City, Vietnam*

Abstract

We study the prospect of probing electroweak baryogenesis driven by an extra bottom Yukawa coupling ρ_{bb} in a general two Higgs doublet model via $bg \rightarrow bA \rightarrow bt\bar{t}$ process, where A is CP odd scalar. The process induced by ρ_{bb} coupling and can be discovered at the high luminosity LHC if $|\rho_{bb}| \sim 0.15$ and, an extra top Yukawa coupling is around 0.5 for $360 \text{ GeV} \lesssim m_A \lesssim 520 \text{ GeV}$, whereas its evidence could be found up to $m_A \sim 600 \text{ GeV}$. We find that the CP asymmetry of inclusive $B \rightarrow X_s \gamma$ decay and the electron electric dipole moment measurement would provide complementary probes for the parameter space. We also study $gg \rightarrow t\bar{t}A \rightarrow t\bar{t}b\bar{b}$ for $m_A < 2m_t$, where m_t is the mass of the top quark and find it not promising.

I. INTRODUCTION

The existence of the matter-antimatter asymmetry is unswervingly established over the years by various cosmological observations such as the cosmic microwave background anisotropies and big-bang nucleosynthesis [1]. It has been understood that the Universe started with equal number of baryons and antibaryons, but later evolved into baryon dominated Universe dynamically via a mechanism called baryogenesis. A successful baryogenesis requires three necessary conditions namely, baryon number violation, charge conjugation (C) and charge conjugation-parity (CP) violation and, departure from thermal equilibrium, laid out by Sakharov in 1967 [2]. A plethora of baryogenesis scenarios have been proposed so far to account for the observed baryon asymmetry of the Universe (BAU), however, its origin is still unclear. After the discovery of the 125 GeV Higgs boson at the Large Hadron Collider (LHC) [3], a significant attention has been directed in particular to electroweak baryogenesis (EWBG) [4–12] mechanism for its direct connections to Higgs physics and, its testability at the ongoing experiments. The Standard Model (SM) belongs to this class, however the CP violation is too small and, the electroweak symmetry breaking is not strongly first order phase transition (EWPT) to drive departure from thermal equilibrium.

While we do not have any strong experimental evidence of new physics yet, multi-Higgs sector is the natural consequence of most ultraviolet (UV) theories due to enlarged symmetries. Whatever the fundamental theory might be, their effective descriptions at $\mathcal{O}(100)$ GeV scale should resemble the SM in light of the latest experimental results. As for the Higgs sector, two cases are conceivable: one is that all the new scalars are much heavier than $\mathcal{O}(100)$ GeV scale, thereby the Higgs sector is effectively reduced to the SM, while the other is that new scalars have $\mathcal{O}(100)$ GeV masses but their couplings to the gauge bosons and fermions are SM like, mimicking the SM. From the viewpoint of new physics discovery potential, it is timely to consider the latter case and investigate whether the aforementioned cosmological issue can be solved or not. Since we have already confirmed the existence of the Higgs doublet in nature, it is tempting to us to think of additional Higgs doublets in analogy with the fact that all the fermions come in three copies.

The general two Higgs doublet model (g2HDM) is one of the simplest renormalizable low-energy models where the scalar sector of the SM is extended by an extra scalar doublet [13]. Without the presence of discrete symmetry, in g2HDM, both the scalar doublets couple with

up- and down-type fermions at tree level. In the mass eigenbasis of the fermions (F), one has two independent Yukawa couplings λ_{ij}^F and ρ_{ij}^F , where the former is real and diagonal that are responsible for the fermion mass generation, while the latter is complex and non-diagonal. Such complex couplings can provide additional CP violating sources beyond the usual Cabibbo-Kobayashi-Maskawa (CKM) framework [14] of the SM.

EWBG in g2HDM is widely investigated in Refs. [8–11]. This model can simultaneously accommodate the strong first-order EWPT and sufficient amount of CP violation which the SM fails to provide. The most natural EWBG scenario in g2HDM would be the case in which BAU is driven by the extra top Yukawa coupling (ρ_{tt}) of $\mathcal{O}(0.01 - 1)$ in magnitude with moderate size of the CP phase (ρ_{tt} -EWBG) [9]. The devoted collider study of this scenario is conducted in Ref. [15].

As a complementary study to ρ_{tt} -EWBG, the present authors consider a scenario in which the CP phase of ρ_{tt} is approximately zero and the extra bottom Yukawa coupling (ρ_{bb}) plays a dominant role in generating BAU (ρ_{bb} -EWBG) [10]. It is demonstrated that BAU can reach the observed level if $|\text{Im}\rho_{bb}| \gtrsim 0.058$ with generous assumptions on a Higgs bubble wall profile.

The ρ_{bb} -EWBG can be discovered at the LHC via $bg \rightarrow bA \rightarrow bZH$ (or $bg \rightarrow bH \rightarrow bZA$) process if $|\text{Im}(\rho_{bb})| \sim \mathcal{O}(0.1)$ [16]. The process however requires $m_A > m_H + m_Z$ and, ρ_{tt} to be negligibly small to avoid constraints from flavor physics [16]. In addition, for $m_A > 2m_t$, the process gets dilution from $A \rightarrow t\bar{t}$ decay if ρ_{tt} non-vanishing. In such a scenario, where both ρ_{bb} and ρ_{tt} are non-zero, one has $bg \rightarrow bA \rightarrow btt$ process (conjugate process implied) for $m_A > 2m_t$. In this paper we study the prospect of probing ρ_{bb} -EWBG mechanism via $bg \rightarrow bA \rightarrow btt$ process at the 14 TeV LHC. Therefore, the process provides unique probe for the parameter space of ρ_{bb} -EWBG mechanism complementary to Ref. [16].

We analyze the discovery prospect of $bg \rightarrow bA \rightarrow btt$ process via $pp \rightarrow bA + X \rightarrow btt + X$ at 14 TeV LHC, where X is inclusive activities. In this paper we study this process where at least one top decays semileptonically, constituting three b -tagged jets, at least one charged lepton (e and μ) and some missing transverse energy signature (denoted as $3b1\ell$ process) for few benchmark masses of A ranging from 400 GeV to 600 GeV. The process provides a sensitive probe for ρ_{bb} -EWBG if $m_A > 2m_t$ and, ρ_{tt} is non-zero. Although a discovery of $bg \rightarrow bA \rightarrow btt$ is possible, however, the information of the phase is beyond the scope of the LHC. The phase information of ρ_{bb} can be probed via the CP asymmetry of $B \rightarrow X_s \gamma$ decay

or via electron electric dipole moment (EDM) measurements.

We also investigate the discovery prospect of $gg \rightarrow t\bar{t}A \rightarrow t\bar{t}b\bar{b}$ for $m_A < 2m_t$ process for completeness. The process is also induced by ρ_{bb} and ρ_{tt} and can probe the parameter space of ρ_{bb} -EWBG below $m_A < 2m_t$. At the LHC the process can be searched via $pp \rightarrow t\bar{t}A + X \rightarrow t\bar{t}b\bar{b} + X$, with at least one top decaying semileptonically.

In the following, we outlined the formalism in Sec. II, followed by a detailed discussion on the available parameter space in Sec. III. We discuss the discovery potential of $bg \rightarrow bA \rightarrow bt\bar{t}$ process in Sec. IV and the $gg \rightarrow t\bar{t}A \rightarrow t\bar{t}b\bar{b}$ process in Sec. V and, summarize our results in Sec. VI with some outlook.

II. FRAMEWORK

The particle content of g2HDM is the SM plus additional Higgs doublet. In general, this model induces flavor-changing neutral current (FCNC) processes mediated by the neutral Higgs bosons at tree level. It is common to impose a Z_2 symmetry to suppress the FCNC processes to be consistent with various flavor physics data. Though this setup works well, having the Z_2 symmetry implies that the model has some specific UV theories such as supersymmetric models. Since we do not try to connect the model to any specific UV completions, we do not impose the Z_2 symmetry or something similar, which enables us to discuss physics at $\mathcal{O}(100)$ GeV scale in wider perspective. In this bottom-up approach, the tree-level FCNC processes are possible as long as the experimental data allow, and sources of CP violation are much richer than 2HDMs with some discrete symmetries.

The most general two Higgs doublet potential can be written in the Higgs basis as [17, 18]

$$V(\Phi, \Phi') = \mu_{11}^2 |\Phi|^2 + \mu_{22}^2 |\Phi'|^2 - (\mu_{12}^2 \Phi^\dagger \Phi' + \text{H.c.}) + \frac{\eta_1}{2} |\Phi|^4 + \frac{\eta_2}{2} |\Phi'|^4 + \eta_3 |\Phi|^2 |\Phi'|^2 + \eta_4 |\Phi^\dagger \Phi'|^2 + \left[\frac{\eta_5}{2} (\Phi^\dagger \Phi')^2 + (\eta_6 |\Phi|^2 + \eta_7 |\Phi'|^2) \Phi^\dagger \Phi' + \text{H.c.} \right]. \quad (1)$$

Each Higgs doublet fields is expressed as

$$\Phi = \begin{pmatrix} G^+ \\ \frac{1}{\sqrt{2}}(v + h + iG^0) \end{pmatrix}, \quad \Phi' = \begin{pmatrix} H^+ \\ \frac{1}{\sqrt{2}}(A + H) \end{pmatrix}, \quad (2)$$

where $v (\simeq 246 \text{ GeV})$ is the the vacuum expectation value, h is the SM-like Higgs boson, $G^{0,\pm}$ are the Nambu-Goldstone bosons, H and A are the CP-even and -odd Higgs bosons,

respectively, and H^\pm are the charged Higgs bosons. From the minimization condition with respect to Φ , it follows that $\mu_{11}^2 = -\eta_1 v^2/2$. For simplicity, we assume CP-conserving Higgs sector at tree level.¹ The second minimization condition with respect to Φ' gives $\mu_{12}^2 = \eta_6 v^2/2$.

The mixing angle γ between the CP-even bosons h and H satisfies the relations [18]

$$\cos^2 \gamma = \frac{\eta_1 v^2 - m_h^2}{m_H^2 - m_h^2}, \quad \sin 2\gamma = \frac{2\eta_6 v^2}{m_H^2 - m_h^2}. \quad (3)$$

An alignment limit is defined as $c_\gamma = 0$ and $s_\gamma = -1$, where c_γ and s_γ are shorthands for $\cos \gamma$ and $\sin \gamma$ respectively. One can express the masses of h , H , A and H^\pm in terms of the parameters in Eq. (1):

$$m_{h,H}^2 = \frac{1}{2} \left[m_A^2 + (\eta_1 + \eta_5) v^2 \mp \sqrt{[m_A^2 + (\eta_5 - \eta_1) v^2]^2 + 4\eta_6^2 v^4} \right], \quad (4)$$

$$m_A^2 = \frac{1}{2} (\eta_3 + \eta_4 - \eta_5) v^2 + \mu_{22}^2, \quad (5)$$

$$m_{H^\pm}^2 = \frac{1}{2} \eta_3 v^2 + \mu_{22}^2. \quad (6)$$

Note that in the alignment limit, one has $m_h^2 = \eta_1 v^2$ and $m_H^2 = m_A^2 + \eta_5 v^2 = (\eta_3 + \eta_4 + \eta_5) v^2/2 + \mu_{22}^2$. In contrast to m_h , the masses of the extra Higgs bosons are controlled by $\eta_i v^2$ and μ_{22}^2 , where η_i denotes some linear combinations of the η couplings. As is well known, magnitudes of the heavy Higgs loop contributions can become sizable if $\eta_i v^2 \gtrsim \mu_{22}^2$, which is necessary for achieving the strong first-order EWPT.

The CP-even scalars h , H and CP-odd scalar A couple to fermions by [17]

$$\begin{aligned} \mathcal{L} = & -\frac{1}{\sqrt{2}} \sum_{F=U,D,L} \bar{F}_i \left[(-\lambda_{ij}^F s_\gamma + \rho_{ij}^F c_\gamma) h + (\lambda_{ij}^F c_\gamma + \rho_{ij}^F s_\gamma) H - i \operatorname{sgn}(Q_F) \rho_{ij}^F A \right] P_R F_j \\ & - \bar{U}_i [(V \rho^D)_{ij} P_R - (\rho^{U^\dagger V})_{ij} P_L] D_j H^- \bar{\nu}_i \rho_{ij}^L P_R L_j H^+ + \text{H.c.}, \end{aligned} \quad (7)$$

where $P_{L,R} \equiv (1 \mp \gamma_5)/2$, $i, j = 1, 2, 3$ are generation indices, V is CKM matrix, and $U = (u, c, t)$, $D = (d, s, b)$, $L = (e, \mu, \tau)$ and $\nu = (\nu_e, \nu_\mu, \nu_\tau)$ are in vectors in flavor space. The matrices λ_{ij}^F ($= \sqrt{2} m_i^F/v$) are real and diagonal, whereas ρ_{ij}^F are in general complex and non-diagonal.

¹ Since we have CP violation in the Yukawa sector as delineated below, its effect appears in the Higgs spectrum at one-loop level and CP-even and -odd Higgs boson mix with each other. Nevertheless, such a one-loop induced mixing is so small that $\{h, H, A\}$ can be regarded as the mass eigenstates to a good approximation.

Our purpose is to study the discovery potential of $bg \rightarrow bA \rightarrow bt\bar{t}$ process and, utilize it as a probe for EWBG driven by extra bottom Yukawa ρ_{bb} . It is found that a successful EWBG requires $|\text{Im}(\rho_{bb})| \gtrsim 0.058$ [10] and can be discovered at the 14 TeV LHC via $bg \rightarrow bA \rightarrow bZH$ process [16]. However the discovery possibility of this process alleviates unless ρ_{tt} is negligibly small, specially for $m_A > 2m_t$. In this paper we focus on probing ρ_{bb} -EWBG mechanism for the parameter space where $|\text{Im}(\rho_{bb})|$ is moderately large $\sim \mathcal{O}(0.1)$ and, $\rho_{tt} \sim \mathcal{O}(1)$ and, $m_A > 2m_t$. We shall see shortly that these values are well allowed by current data. The process also requires $m_A > 2m_t$. For non-zero $|\text{Im}(\rho_{bb})|$ and ρ_{tt} one has $bg \rightarrow bA \rightarrow bt\bar{t}$, which can be searched at the LHC via $pp \rightarrow bA + X \rightarrow bt\bar{t} + X$ process. One also has $gg \rightarrow t\bar{t}A \rightarrow t\bar{t}b\bar{b}$ [19, 20] which can probe ρ_{bb} -EWBG specially for $m_A < 2m_t$. However, we would show in Sec. V that the process is not so promising and, primarily focus on $bg \rightarrow bA \rightarrow bt\bar{t}$ process. Note that ρ_{bb} and ρ_{tt} would also induce $bg \rightarrow bH \rightarrow bt\bar{t}$, where a similar strategy can be followed.

The complex non-zero ρ_{tt} provides a more robust mechanism for EWBG [9, 11]. Therefore, $bg \rightarrow bA \rightarrow bt\bar{t}$ process would also provide complementary information to EWBG induced by extra top Yukawa ρ_{tt} . We also remark that for non-vanishing ρ_{bb} and ρ_{tt} one may also have $gg \rightarrow b\bar{b}A/H \rightarrow b\bar{b}t\bar{t}$, which are covered in Refs. [19, 20]. Indeed, non-zero ρ_{tt} motivates the conventional $gg \rightarrow H \rightarrow t\bar{t}$ [21, 22] (see also [23]) search or, $gg \rightarrow t\bar{t}A/H \rightarrow t\bar{t}t\bar{t}$ [19, 20, 24] i.e., the four top search. Though the former process suffers from large interference with the overwhelming QCD $gg \rightarrow t\bar{t}$ background [23], recent searches performed by both ATLAS [21] and CMS [22] find some sensitivity.

III. PARAMETER SPACE

Let us focus on the allowed parameter space for the $bg \rightarrow bA \rightarrow bt\bar{t}$ process, for which the mass of A should be heavier than $2m_t$. To explore whether such a mass spectrum exists, the parameters in Eq. (1) are required to satisfy perturbativity, tree-level unitarity and vacuum stability conditions, for which we utilized the public tool 2HDMC [25]. We express the

quartic couplings η_1, η_{3-6} in terms of $m_h, m_H, m_{H^\pm}, m_A, \mu_{22}, \gamma$, and v as [17]

$$\eta_1 = \frac{m_h^2 s_\gamma^2 + m_H^2 c_\gamma^2}{v^2}, \quad (8)$$

$$\eta_3 = \frac{2(m_{H^\pm}^2 - \mu_{22}^2)}{v^2}, \quad (9)$$

$$\eta_4 = \frac{m_h^2 c_\gamma^2 + m_H^2 s_\gamma^2 - 2m_{H^\pm}^2 + m_A^2}{v^2}, \quad (10)$$

$$\eta_5 = \frac{m_H^2 s_\gamma^2 + m_h^2 c_\gamma^2 - m_A^2}{v^2}, \quad (11)$$

$$\eta_6 = \frac{(m_h^2 - m_H^2)(-s_\gamma)c_\gamma}{v^2}. \quad (12)$$

The quartic couplings η_2 and η_7 do not enter scalar masses, nor the mixing angle γ . Therefore in our analysis we take v, m_h , and $\gamma, m_A, m_H, m_{H^\pm}, \mu_{22}, \eta_2, \eta_7$ as the phenomenological parameters. Further, to save computation time, we randomly generated these parameters for $m_{H^\pm} = 300$ GeV and 500 GeV in the following ranges: $\mu_{22} \in [0, 1000]$ GeV, $m_A \in [350, 800]$ GeV, $m_H \in [350, 800]$ GeV, $m_{H^\pm} \in [350, 800]$ GeV, $\eta_2 \in [0, 3]$, $\eta_7 \in [-3, 3]$, while satisfying $m_h = 125$ GeV. We remark that, since the $bg \rightarrow bA \rightarrow bt\bar{t}$ process does not depend on c_γ , for simplicity we assumed $c_\gamma = 0$. This also help us to avoid several minor constraints.² The randomly generated parameters are then fed into 2HDMC for scanning. 2HDMC utilizes [25] m_{H^\pm} and Λ_{1-7} as the input parameters in the Higgs basis whereas $v \simeq 246$ GeV. In order to match the 2HDMC convention, we identify η_{1-7} as Λ_{1-7} and, take $-\pi/2 \leq \gamma \leq \pi/2$. For the positivity conditions of the Higgs potential of Eq. (1), the parameter $\eta_2 > 0$ along with other more involved conditions implemented in 2HDMC. We further conservatively demand $|\eta_i| \leq 3$.

Next we impose the stringent oblique T parameter [26] constraint, which restricts hierarchical structures among the scalar masses m_H, m_A and m_{H^\pm} [27, 28], and hence η_i s. Utilizing the expression given in Ref. [28] the points that passed unitarity, perturbativity and positivity conditions from 2HDMC, are further required to satisfy the T parameter constraint within the 2σ error [29]. These points are denoted as “scanned points”. We plot the scanned points in the m_A – m_H and m_A – m_{H^\pm} planes in the left and right panels of Fig. 1, which illustrates that significant amounts of the allowed points exists. A more detailed discussions on the scanning procedure can be found in Refs. [30, 31].

² Note that, for successful ρ_{bb} induced EWBG, one requires non vanishing c_γ as discussed in Ref. [10]. It was shown that for $c_\gamma \sim 0.1$, current data still allows $\text{Im}(\rho_{bb}) \sim 0.15$ – 0.2 , while $|\text{Im}(\rho_{bb})| \gtrsim 0.058$ is sufficient to account for the observed BAU [10]. We stress that we set $c_\gamma = 0$ to avoid some inconsequential constraints which has no real impact on the discovery of $bg \rightarrow bA \rightarrow bt\bar{t}$ process.

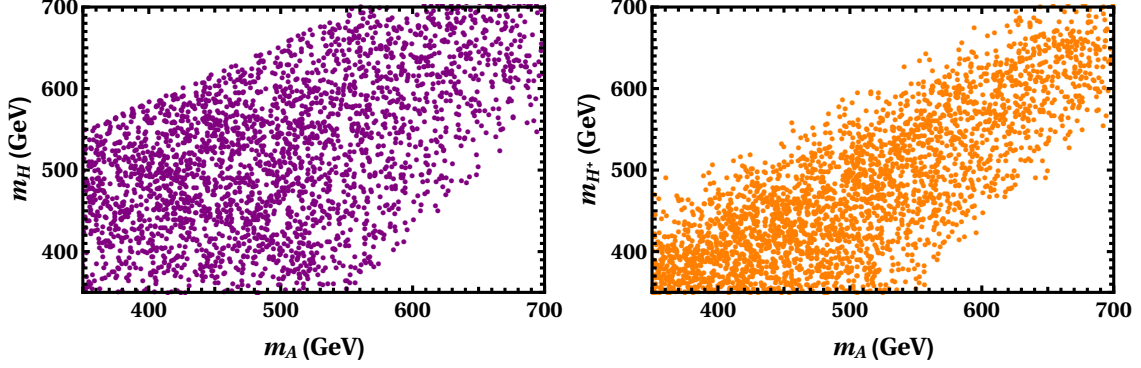


FIG. 1. Scanned points plotted in m_A - m_H (left) and m_A - m_{H^\pm} (right) plane. Here the scanned points satisfy the tree level unitarity, perturbativity and positivity conditions as well as the T parameter constraint.

BP	η_1	η_2	η_3	η_4	η_5	η_6	η_7	m_{H^\pm} (GeV)	m_A (GeV)	m_H (GeV)	$\frac{\mu_{22}^2}{v^2}$
<i>a</i>	0.258	1.786	2.449	-0.957	2.09	0	0.118	512	412	544	3.1
<i>b</i>	0.258	2.134	2.836	-0.402	2.565	0	-1.647	597	516	649	4.45
<i>c</i>	0.258	2.379	2.86	-0.193	2.78	0	0.625	657	585	715	5.7

TABLE I. Parameter values of three benchmark points chosen from the scanned points in Fig. 1 for $m_A > 2m_t$.

To find the constraints on ρ_{bb} and ρ_{tt} and, subsequently analyze the discovery potential of $bg \rightarrow bA \rightarrow bt\bar{t}$ process, we choose three benchmark points (BPs) from the scanned points which are summarized in Table I. For BP*a*, we choose $m_A \sim 400$ GeV i.e., just above $2m_t$ threshold, whereas, for BP*b* and BP*c*, $m_A \sim 500$ GeV and $m_A \sim 600$ GeV respectively. Further, for all three BPs, A is assumed to be lighter than H and H^\pm to suppress $A \rightarrow ZH$ and $A \rightarrow H^\pm W^\mp$ decays. Such an assumption boosts the discovery potential of $bg \rightarrow bA \rightarrow bt\bar{t}$ process to some extent. Heavier A are indeed possible, but, the cross sections are reduced due to rapid fall in the parton luminosity. We also remark that one requires [4] sub-TeV m_A , m_{H^\pm} and m_H for the strong first-order EWPT, which is required for conventional sub-TeV EWBG [5–7] (for high-scale EWBG, see, e.g., Refs. [12]).

In the following we will scrutinize the relevant constraints on ρ_{bb} and ρ_{tt} . For simplicity,

we assume that ρ_{ij} except for ρ_{bb} , ρ_{tt} and ρ_{ee} are negligibly small so as not to affect our main discussion. The impacts of non-zero ρ_{ij} would be discussed later part of the paper.

A. Flavor Constraints

There exist several constraints from flavor physics that restricts the parameter space. In particular, the following three observables are relevant: (i) the branching ratio measurement of $B \rightarrow X_s \gamma$ ($\mathcal{B}(B \rightarrow X_s \gamma)$), (ii) the asymmetry of the CP asymmetry between the charged and neutral $B \rightarrow X_s \gamma$ decays ($\Delta\mathcal{A}_{\text{CP}}$) and (iii) the $B_q\text{-}\overline{B}_q$ ($q = d, s$) mixings.

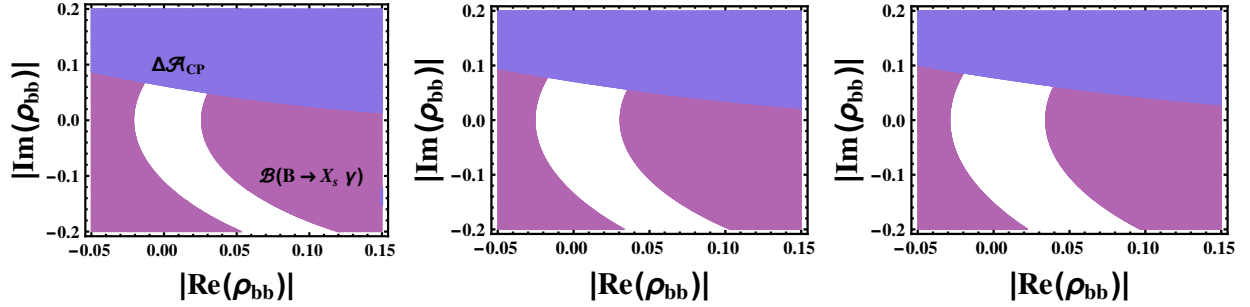


FIG. 2. The constraints on ρ_{bb} from $\mathcal{B}(B \rightarrow X_s \gamma)$ (purple) and $\Delta\mathcal{A}_{\text{CP}}$ (blue) measurements for the BP a (left), BP b (middle) and BP c (right) respectively. All three figures are generated assuming $\rho_{tt} = 0.5$. See text for details.

Let us first focus on $\mathcal{B}(B \rightarrow X_s \gamma)$. Non-zero ρ_{bb} and ρ_{tt} modify $\mathcal{B}(B \rightarrow X_s \gamma)$ via top quark and charged Higgs boson loop. The modification is parametrized by the (LO) Wilson coefficients $C_{7,8}^{(0)}$ at the matching scale $\mu = m_W$

$$C_{7,8}^{(0)}(m_W) = F_{7,8}^{(1)}(x_t) + \delta C_{7,8}^{(0)}(\mu_W), \quad (13)$$

where, $\overline{m}_t(m_W)$ is the top quark $\overline{\text{MS}}$ running mass at the m_W scale with $x_t = (\overline{m}_t(m_W)/m_W)^2$. The expression for $F_{7,8}^{(1)}(x)$ can be found in the Refs. [32, 33], whereas $\delta C_{7,8}^{(0)}(\mu_W)$ the LO (leading order) charged Higgs contributions. At LO, $\delta C_{7,8}^{(0)}(\mu_W)$ is expressed as [34]

$$\delta C_{7,8}^{(0)}(m_W) \simeq \frac{|\rho_{tt}|^2}{3\lambda_t^2} F_{7,8}^{(1)}(y_{H^+}) - \frac{\rho_{tt}\rho_{bb}}{\lambda_t\lambda_b} F_{7,8}^{(2)}(y_{H^+}), \quad (14)$$

with $y_{H^+} = (\overline{m}_t(m_W)/m_{H^+})^2$ while, the full expression for $F_{7,8}^{(2)}(y_{H^+})$ can be found in Ref. [32]. The current world average of $\mathcal{B}(B \rightarrow X_s \gamma)_{\text{exp}}$ extrapolated to the photon-energy

cut $E_0 = 1.6$ GeV is found by the HFLAV Collaboration to be $(3.32 \pm 0.15) \times 10^{-4}$ [35]. The next-to-next-to LO (NNLO) $\mathcal{B}(B \rightarrow X_s \gamma)$ prediction in the SM for the same photon-energy cut is $(3.36 \pm 0.23) \times 10^{-4}$ [36]. In order to find the constraint, we adopt the prescription outlined in Ref. [37] and define

$$R_{\text{exp}} = \frac{\mathcal{B}(B \rightarrow X_s \gamma)_{\text{exp}}}{\mathcal{B}(B \rightarrow X_s \gamma)_{\text{SM}}}. \quad (15)$$

Based on our LO Wilson coefficients, we further express

$$R_{\text{theory}} = \frac{\mathcal{B}(B \rightarrow X_s \gamma)_{\text{g2HDM}}}{\mathcal{B}(B \rightarrow X_s \gamma)_{\text{SM}}}, \quad (16)$$

and take m_W and $\bar{m}_b(m_b)$ respectively as the matching scale and the low-energy scales. Finally, we demand R_{theory} to remain within the 2σ error of R_{exp} . In Fig. 2 the excluded regions are shown as the purple shaded regions in the $\text{Re}(\rho_{bb})$ – $\text{Im}(\rho_{bb})$ plane for three BPs. Here, we assume $\rho_{tt} = 0.5$. Flavor constraints on ρ_{tt} is moderately strong, with $B_{d,s}$ – $\bar{B}_{d,s}$ mixings providing the most stringent constraint on ρ_{tt} for $500 \lesssim m_{H^\pm} \lesssim 650$ GeV, which is the ballpark mass ranges of m_{H^\pm} for all the three BPs. The B_q – \bar{B}_q mixing amplitude M_{12}^q receives modification from the charged Higgs and W bosons loop with t quark. Utilizing the expression for B_q – \bar{B}_q mixing in type-II 2HDM [38], it is found in Ref. [34] that

$$\frac{M_{12}^q}{M_{12}^{q\text{SM}}} = 1 + \frac{I_{WH}(y_W, y_H, x) + I_{HH}(y_H)}{I_{WW}(y_W)}, \quad (17)$$

where $y_i = m_t^2/m_i^2$ ($i = W, H^\pm$) and $x = m_{H^\pm}^2/m_W^2$ with m_t and m_W being the masses of the top quark and W bosons. The expressions for I_{WW} , I_{WH} and I_{HH} are respectively given by [34]

$$I_{WW} = 1 + \frac{9}{1 - y_W} - \frac{6}{(1 - y_W)^2} - \frac{6}{y_W} \left(\frac{y_W}{1 - y_W} \right)^3 \ln y_W, \quad (18)$$

$$I_{WH} \simeq \left(\frac{\rho_{tt}^*}{\lambda_t} + \frac{V_{cb}\rho_{ct}^*}{V_{tb}\lambda_t} \right) \left(\frac{\rho_{tt}}{\lambda_t} + \frac{V_{cq}\rho_{ct}}{V_{tq}\lambda_t} \right) y_H \\ \times \left[\frac{(2x - 8) \ln y_H}{(1 - x)(1 - y_H)^2} + \frac{6x \ln y_W}{(1 - x)(1 - y_W)^2} - \frac{8 - 2y_W}{(1 - y_W)(1 - y_H)} \right], \quad (19)$$

$$I_{HH} \simeq \left(\frac{\rho_{tt}^*}{\lambda_t} + \frac{V_{cb}\rho_{ct}^*}{V_{tb}\lambda_t} \right)^2 \left(\frac{\rho_{tt}}{\lambda_t} + \frac{V_{cq}\rho_{ct}}{V_{tq}\lambda_t} \right)^2 \left(\frac{1 + y_H}{(1 - y_H)^2} + \frac{2y_H \ln y_H}{(1 - y_H)^3} \right) y_H. \quad (20)$$

For $|\rho_{tt}| \sim \mathcal{O}(1)$ coupling ρ_{ct} is strongly constrained due to $|V_{cq}/V_{tq}| \sim 25$ ($q = d, s$) enhancement [34], as can be seen from Eqs.(19) and (20). As we are primarily interested in

the parameter space where ρ_{tt} is $\mathcal{O}(1)$, we turn off ρ_{ct} throughout our paper for simplicity. The 2018 summer results of UTfit finds [39]:

$$\begin{aligned} C_{B_d} &\in 1.05 \pm 0.11, \\ C_{B_s} &\in 1.110 \pm 0.090, \\ \phi_{B_d} &\in -2.0 \pm 1.8 \text{ [in } ^\circ], \\ \phi_{B_s} &\in 0.42 \pm 0.89 \text{ [in } ^\circ]. \end{aligned} \tag{21}$$

with $M_{12}^q/M^{q\text{ SM}} = C_{B_q} e^{2i\phi_{B_q}}$. Under the assumption on the ρ_{ij}^F couplings made in our analysis, we have $M_{12}^q/M^{q\text{ SM}} = C_{B_q}$. Allowing 2σ errors on C_{B_d} and C_{B_s} we find that $B_{s,d}-\bar{B}_{d,s}$ mixings exclude $|\rho_{tt}| \gtrsim 1.1$ for BPa and $|\rho_{tt}| \gtrsim 1.2$ for BPb and BPC.

One of the most powerful probes of $\text{Im}(\rho_{bb})$ is the direct CP asymmetry \mathcal{A}_{CP} [40] of $B \rightarrow X_s \gamma$. It is advocated in Ref. [41], however, that $\Delta\mathcal{A}_{\text{CP}}$ is even more sensitive to the CP-violating couplings, which is defined as [41]

$$\Delta\mathcal{A}_{\text{CP}} = \mathcal{A}_{B^- \rightarrow X_s^- \gamma} - \mathcal{A}_{B^0 \rightarrow X_s^0 \gamma} \approx 4\pi^2 \alpha_s \frac{\tilde{\Lambda}_{78}}{m_b} \text{Im}\left(\frac{C_8}{C_7}\right), \tag{22}$$

where $\tilde{\Lambda}_{78}$ and α_s denote a hadronic parameter and the strong coupling constant at $\bar{m}_b(m_b)$ scale, respectively. One expects that $\tilde{\Lambda}_{78}$ has a similar scale of Λ_{QCD} . In Ref. [41], it is found that $17 \text{ MeV} \leq \tilde{\Lambda}_{78} \leq 190 \text{ MeV}$. On the other hand, recently Belle measured $\Delta\mathcal{A}_{\text{CP}} = (+3.69 \pm 2.65 \pm 0.76)\%$ [42], where the first uncertainty is statistical while the second one is systematic. Allowing 2σ error on the Belle measurement, we show the regions excluded by $\Delta\mathcal{A}_{\text{CP}}$ in blue shade in Figs. 2 for the three BPs. Here, we choose the average value of $\tilde{\Lambda}_{78}$ i.e., 89 MeV for illustration. We stress that the constraint shown in Figs. 2 depends heavily on the value of $\tilde{\Lambda}_{78}$. The larger $\tilde{\Lambda}_{78}$ would make the constraint stronger. We also remark that we utilize the LO Wilson coefficients in Eq. (13) as a first approximation for simplicity. Note that the excluded regions by $\Delta\mathcal{A}_{\text{CP}}$ measurement in Fig. 2 is asymmetric and constrains positive $\text{Im}(\rho_{bb})$ more stringently. This is solely due to our choice of $\rho_{tt} = 0.5$. If we take $\rho_{tt} = -0.5$, the blue shaded regions would flip and exclude the negative regions of $\text{Im}(\rho_{bb})$.

We note in passing that if ρ_{tt} is also complex, $\Delta\mathcal{A}_{\text{CP}}$ can be zero if the complex phases of ρ_{tt} and ρ_{bb} are aligned, i.e., $\text{Im}(\rho_{tt}\rho_{bb})=0$, equivalently, $\text{Re}\rho_{bb}/\text{Re}\rho_{tt} = -\text{Im}\rho_{bb}/\text{Im}\rho_{tt}$. Such a phase alignment is discussed in Ref. [11].

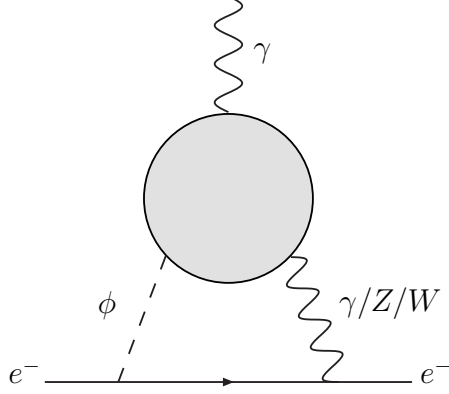


FIG. 3. Two-loop Barr-Zee diagrams contributing to the electron EDM, where $\phi = h, H, A, H^\pm$. The shaded loop collectively represents the scalar, fermion and gauge boson loops. The total contribution is given by their sum, $d_e = d_e^{\phi\gamma} + d_e^{\phi Z} + d_e^{\phi W}$.

B. EDMs

The complex phase of ρ_{bb} is severely constrained by EDMs of the electron, neutron, and atoms, etc. Currently, the most stringent experimental bound comes from EDM of thorium monoxide (ThO), which is approximately given by

$$d_{\text{ThO}} = d_e + \alpha_{\text{ThO}} C_S, \quad (23)$$

where d_e is the electron EDM and C_S is the coefficient of the nuclear spin-independent interaction (NSID), which are respectively defined as

$$\mathcal{L}_{\text{EDM}} = -\frac{i}{2} d_e F^{\mu\nu} \bar{e} \sigma_{\mu\nu} \gamma_5 e, \quad \mathcal{L}_{eN}^{\text{NSID}} = -\frac{G_F}{\sqrt{2}} C_S (\bar{N} N) (\bar{e} i \gamma_5 e), \quad (24)$$

where $F^{\mu\nu}$ denotes the field strength tensor of electromagnetism and G_F is the Fermi coupling constant. The coefficient α_{ThO} is estimated as $\alpha_{\text{ThO}} = 1.5 \times 10^{-20}$ [43]. The latest experimental value of d_{ThO} is placed by ACME Collaboration in 2018 (ACME18) as

$$d_{\text{ThO}} = (4.3 \pm 4.0) \times 10^{-30} \text{ e cm}, \quad (25)$$

from which under the assumption of $C_S = 0$ the electron EDM has an upper bound of

$$|d_e| < 1.1 \times 10^{-29} \text{ e cm}. \quad (26)$$

In our scenario, d_e is predominantly induced by two-loop Barr-Zee diagrams as depicted in Fig. 3, which are decomposed into the three parts:

$$d_e = d_e^{\phi\gamma} + d_e^{\phi Z} + d_e^{\phi W}, \quad (27)$$

where $\phi = h, H, A$ for the first two terms and $\phi = H^\pm$ for the last term. Let us denote the contribution of i -species to $d_e^{\phi\gamma}$ as $(d_e^{\phi\gamma})_i$. If ρ_{bb} is the only source of CP violation, $d_e \simeq (d_e^{\phi\gamma})_b$. With $\text{Im}\rho_{bb}$ required by ρ_{bb} -EWBG mechanism, d_e is so large that one cannot avoid the ACME18 bound as noted in Ref. [10]. This fact suggests two options: (i) the alignment limit ($c_\gamma \rightarrow 0$) and (ii) cancellation mechanism. As discussed in Ref. [11], however, the first option may not be consistent with EWBG in g2HDM since the BAU would be suppressed with decreasing c_γ . We thus consider the second option. Even though we identify the parameter space for the cancellation in Ref. [10], we do not show its detail there, and moreover, $d_e^{\phi W}$, which can come into play in the cancellation region, is missing. We therefore update our previous analysis taking all the relevant contributions into consideration.

If there exist more than two CP -violating phases, we could tune the parameters in such a way that d_e becomes small. While it is nothing more than the parameter turning, we still classify the cancellation parameter space into two kind. We call a cancellation *structured cancellation* if it happens when the hierarchical structures of the ρ_{ij} matrices closely resemble those of the SM Yukawa matrices, and anything else is *unstructured cancellation*. It is revealed in Ref. [11] that the parameter space of ρ_{tt} -EWBG accommodates the structured cancellation. We here scrutinize the type of the cancellation in ρ_{bb} -EWBG.

Following a method adopted in Ref. [11], we split $(d_e^{\phi\gamma})_b$ into two parts as³

$$(d_e^{\phi\gamma})_f = (d_e^{\phi\gamma})_f^{\text{mix}} + (d_e^{\phi\gamma})_f^{\text{extr}}, \quad (28)$$

where

$$\frac{(d_e^{\phi\gamma})_f^{\text{mix}}}{e} = -\frac{3\alpha_{\text{em}}Q_f^2s_{2\gamma}}{16\sqrt{2}\pi^3v} \left[\text{Im}(\rho_{ee})\Delta f_f + \frac{\lambda_e}{\lambda_f} \text{Im}(\rho_{ff})\Delta g_f \right], \quad (29)$$

$$\begin{aligned} \frac{(d_e^{\phi\gamma})_f^{\text{extr}}}{e} = & \frac{3\alpha_{\text{em}}Q_f^2}{16\pi^3m_f} \left[\text{Im}(\rho_{ee})\text{Re}(\rho_{ff}) \left\{ c_\gamma^2 f(\tau_{fh}) + s_\gamma^2 f(\tau_{fH}) \pm g(\tau_{fA}) \right\} \right. \\ & \left. + \text{Im}(\rho_{ff})\text{Re}(\rho_{ee}) \left\{ c_\gamma^2 g(\tau_{fh}) + s_\gamma^2 g(\tau_{fH}) \pm f(\tau_{fA}) \right\} \right], \quad (30) \end{aligned}$$

with α_{em} and Q_f representing the fine structure constant and electric charges of f , respectively, and $\Delta f_f = f(\tau_{fh}) - f(\tau_{fH})$ and $\Delta g_f = g(\tau_{fh}) - g(\tau_{fH})$ with $\tau_{ij} = m_i^2/m_j^2$. $f(\tau)$ and $g(\tau)$ are the loop functions and their explicit forms are shown in Appendix A. In our notation, the sign of e is positive. In the wave parenthesis in Eq. (30), the upper sign is

³ By convention in this paper, the sign of γ is opposite to that in Ref. [11].

for up-type fermions and the lower is for down-type fermions, respectively. For $c_\gamma \ll 1$ and $m_H \simeq m_A$, $(d_e^{\phi\gamma})_{t,b}^{\text{extr}}$ are approximated as

$$\frac{(d_e^{H\gamma})_t^{\text{extr}}}{e} \simeq \frac{\alpha_{\text{em}}}{12\pi^3 m_t} \text{Im}(\rho_{ee}\rho_{tt}) \left[f(\tau_{tH}) + g(\tau_{tH}) \right], \quad (31)$$

$$\frac{(d_e^{H\gamma})_b^{\text{extr}}}{e} \simeq \frac{\alpha_{\text{em}}}{48\pi^3 m_b} \text{Im}(\rho_{ee}\rho_{bb}^*) \left[f(\tau_{bH}) - g(\tau_{bH}) \right]. \quad (32)$$

In the ρ_{bb} -EWBG scenario, $\text{Im}(\rho_{ee}\rho_{tt}) = \rho_{tt}\text{Im}(\rho_{ee})$. To make our discussion on the cancellation mechanism simpler, we consider a case in which $\text{Im}(\rho_{ee}\rho_{bb}^*) \simeq 0$ so that $(d_e^{\phi\gamma})_b \simeq (d_e^{\phi\gamma})_b^{\text{mix}}$. When ρ_{ee} is nonzero, the primary contribution could be $(d_e^{\phi\gamma})_W$ as inferred from the fact that the ϕ - γ - γ vertex in $d_e^{\phi\gamma}$ is more or less common to the $h \rightarrow 2\gamma$ decay. Noting that the W -loop has only the “mix” contribution since the Higgs couplings to the W bosons are the gauge couplings, one may find [44]

$$\frac{(d_e^{H\gamma})_W}{e} = \frac{(d_e^{H\gamma})_W^{\text{mix}}}{e} = \frac{\alpha_{\text{em}} s_{2\gamma}}{64\sqrt{2}\pi^3 v} \text{Im}(\rho_{ee}) \Delta\mathcal{J}_W^\gamma, \quad (33)$$

where $\Delta\mathcal{J}_W^\gamma = \mathcal{J}_W^\gamma(m_h) - \mathcal{J}_W^\gamma(m_H)$ (for explicit form of \mathcal{J}_W^γ , see Appendix A). From the condition of $(d_e^{\phi\gamma})_t + (d_e^{\phi\gamma})_b + (d_e^{\phi\gamma})_W = 0$, it follows that

$$\frac{\text{Im}(\rho_{ee})}{\text{Im}(\rho_{bb})} = -\frac{s_{2\gamma}\Delta g_b/4}{s_{2\gamma}[\Delta f_t + \Delta f_b/4 - (3/16)\Delta\mathcal{J}_W^\gamma] + 2\rho_{tt}[f(\tau_{tH}) + g(\tau_{tH})]/\lambda_t} \equiv -c \times \frac{\lambda_e}{\lambda_b}. \quad (34)$$

It is found that $c = 2.0 \times 10^{-3}$ for $c_\gamma = 0.1$, $\rho_{tt} = 0.5$, $m_h = 125$ GeV and $m_H = 500$ GeV. Therefore, the cancellation is possible but unstructured since c deviates much from the unity as opposed to the ρ_{tt} -EWBG scenario [11]. Once this accidental cancellation happens, other contributions could become relevant. On the grounds of dimensional analysis, one can find that $d_e^{\phi Z}$ is suppressed by the Z boson coupling to the electron, $g_{Zee} = 1/4 - \sin\theta_W \simeq 0.02$ with θ_W representing the weak mixing angle, while $d_e^{\phi W}$ is not and becomes leading contribution. The dominant contribution in $d_e^{\phi W}$ comes from the diagrams involving the top and bottom loops, which amounts to [11, 45]

$$\frac{(d_e^{\phi W})_{t/b}}{e} \simeq \frac{3\alpha_{\text{em}}|V_{tb}|^2}{128\pi^3 s_W^2} \frac{m_t}{m_{H^\pm}^2} \text{Im}(\rho_{ee}\rho_{tt}) J_1(\tau_{WH^\pm}, \tau_{tH^\pm}), \quad (35)$$

where $m_b = 0$ and V_{tb} is the (33) element of the CKM matrix, which is close to one [1]. J_1 is the loop function listed in Appendix A. In general, this contribution has the ρ_{bb} dependence but vanishes in the case of $m_b = 0$. Note that $(d_e^{\phi W})_{t/b}$ is absent in the softly-broken Z_2 2HDMs. For one of the ρ_{bb} -EWBG parameter points, e.g., $\text{Im}(\rho_{bb}) = -0.15$, one would get

$(d_e^{\phi W})_{t/b} \simeq 2.0 \times 10^{-29} e \text{ cm}$ in the cancellation region specified by Eq. (34), together with $m_{H^\pm} = 500 \text{ GeV}$ and $\rho_{tt} = 0.5$, which slightly exceeds the ACME18 bound. Therefore, the allowed region is not exactly determined by the cancellation condition but it occurs in its vicinity, as we show in our numerical analysis conducted below. It should be noted that even though ρ_{tt} is real in ρ_{bb} -EWBG, its magnitude can be constrained by the electron EDM due to the proportionality of $\rho_{tt}\text{Im}(\rho_{ee})$.

Now we move on to discuss the C_S contribution. We estimate C_S using the CP-violating 4-fermion interactions between the quarks and electron defined as

$$\mathcal{L}_{4f}^{\text{CPV}} = \sum_q C_{qe}(\bar{q}q)(\bar{e}i\gamma_5 e), \quad (36)$$

where $C_{qe} = \sum_{\phi=h,H,A} g_{\phi\bar{q}q}^S g_{\phi\bar{e}e}^P / m_\phi^2$ (explicit forms of $g_{\phi\bar{q}q}^S$ and $g_{\phi\bar{e}e}^P$ are shown in Appendix A) With those, C_S is estimated as [46]

$$C_S = -2v^2 \left[6.3(C_{ue} + C_{de}) + C_{se} \frac{41 \text{ MeV}}{m_s} + C_{ce} \frac{79 \text{ MeV}}{m_c} + 62 \text{ MeV} \left(\frac{C_{be}}{m_b} + \frac{C_{te}}{m_t} \right) \right]. \quad (37)$$

Note that for $c_\gamma \ll 1$ and $m_H \simeq m_A$, C_{qe} for up- and down-type quarks are, respectively, cast into the form [11]

$$C_{ue} \simeq \frac{1}{2m_H^2} \text{Im}(\rho_{ee}\rho_{uu}), \quad C_{de} \simeq \frac{1}{2m_H^2} \text{Im}(\rho_{ee}\rho_{dd}^*). \quad (38)$$

Therefore, the dependences of the CP-violating phases are the same as those of $(d_e^{\phi\gamma})_u^{\text{extr}}$ and $(d_e^{\phi\gamma})_d^{\text{extr}}$, respectively.

In our numerical analysis, we parametrize ρ_{ff} , except for ρ_{tt} , as $\text{Re}(\rho_{ee}) = -r(\lambda_e/\lambda_b)\text{Re}(\rho_{bb})$ and $\text{Im}(\rho_{ee}) = -r(\lambda_e/\lambda_b)\text{Im}(\rho_{bb})$. Though the CP-violating phases in the first and second generations of ρ^F matrices have nothing to do with ρ_{bb} -EWBG, we fix them through the above relations. However, the effects of the extra CP violation are too small to affect our cancellation mechanism in ρ_{bb} -EWBG.

In Fig. 4, $|d_{\text{ThO}}|$ and its details are shown as functions of r . We take BP*a* for the Higgs spectrum and set $c_\gamma = 0.1$, $\text{Re}(\rho_{bb}) = 0$, $\text{Im}(\rho_{bb}) = -0.15$ and $\rho_{tt} = 0.5$ as an example of the ρ_{bb} -EWBG scenario. As seen, the magnitude of $\alpha_{\text{ThO}}C_S$ is much smaller than that of d_e , we thus can use the ACME18 bound of $|d_e| < 1.1 \times 10^{-29} e \text{ cm}$, which is represented by the horizontal dotted line in black, to constrain the parameter space. As discussed in Eq. (34), the cancellation happens in $d_e^{\phi\gamma}$ at around $r \simeq 2 \times 10^{-3}$, which is the consequences of $(d_e^{\phi\gamma})_t + (d_e^{\phi\gamma})_b + (d_e^{\phi\gamma})_W \simeq 0$. At this point, $d_e^{\phi W}$ becomes dominant and $|d_e|$ exceeds the

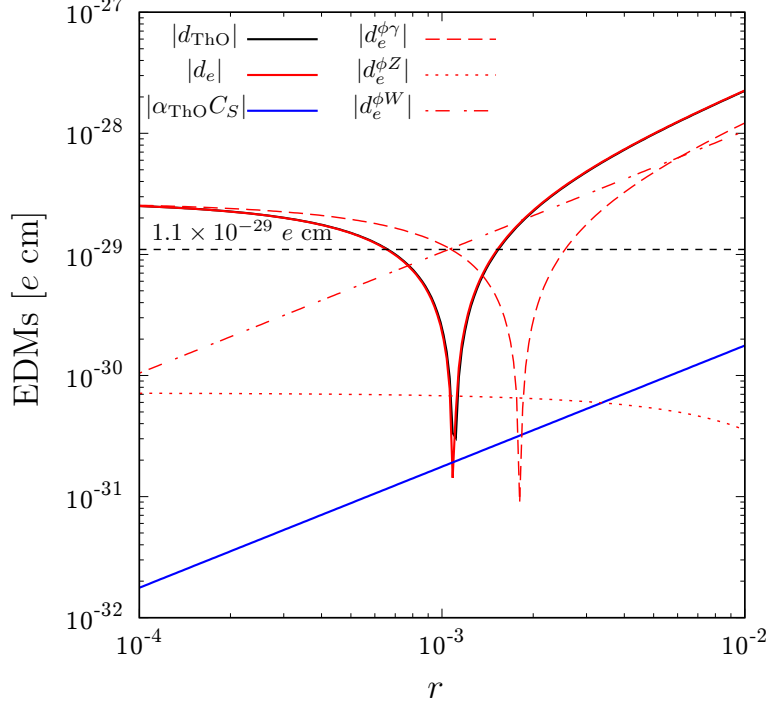


FIG. 4. Details of EDMs as functions of r . We take BP*a* for the Higgs spectrum and set $c_\gamma = 0.1$, $\text{Re}(\rho_{bb}) = 0$, $\text{Im}(\rho_{bb}) = -0.15$ and $\rho_{tt} = 0.5$ as an example of the ρ_{bb} -EWBG scenario. Other ρ_{ff} are fixed by $\text{Re}(\rho_{ee}) = -r(\lambda_e/\lambda_b)\text{Re}(\rho_{bb})$ and $\text{Im}(\rho_{ee}) = -r(\lambda_e/\lambda_b)\text{Im}(\rho_{bb})$. The ACME18 bound ($|d_e| < 1.1 \times 10^{-29} \text{ e cm}$) is shown by the horizontal dotted line in black.

ACME 18 bound. Nevertheless, the cancellation is still at work at around $r \simeq 1 \times 10^{-3}$. Similar to this case, we can always find cancellation regions in the cases of BP*b* and BP*c* as well, and thus conclude that ρ_{bb} -EWBG scenario is still consistent with the ACME18 bound. Note that here we set $c_\gamma = 0.1$ while finding the constraints from ACME18 to illustrate $\text{Im}(\rho_{bb}) \sim 0.15$ is still allowed for $\rho_{tt} \sim 0.5$ for all the three BPs. In the rest of the paper, however, we ignore the c_γ dependence since it is insensitive to our collider study.

Here, we briefly discuss the EDMs of neutron and Mercury. Their current experimental values are respectively given by [47, 48]

$$|d_n| < 1.8 \times 10^{-26} \text{ e cm (90\% C.L.)}, \quad (39)$$

$$|d_{\text{Hg}}| < 7.4 \times 10^{-30} \text{ e cm (95\% C.L.)}. \quad (40)$$

On the theoretical side, the neutron EDM based on QCD sum rules is estimated as [49],

$$d_n = -0.20d_u + 0.78d_d + e(0.29d_u^C + 0.59d_d^C)/g_3, \quad (41)$$

where g_3 is the $SU(3)_C$ gauge coupling and d_q^C are the quark chromo EDMs defined by the operator $\mathcal{L}_{\text{CEDM}} = -(i/2)d_q^C G^{\mu\nu} \bar{q} \sigma_{\mu\nu} \gamma_5 q$ with $G^{\mu\nu}$ representing $SU(3)_C$ field strength tensor. We note that even though the cancellation mechanism can work in d_n as well, it does not occur at the cancellation point of d_e . Using the same input parameters as in Fig. 4 with $r = 10^{-3}$, we obtain $|d_n| = 2.3 \times 10^{-29} e \text{ cm}$, which is nearly 3 orders of magnitude below the current bound. For the mercury EDM, on the other hand, we estimate it using formulas in Refs. [50–52] assuming d_{Hg}^I defined in Ref. [51] and find that $|d_{\text{Hg}}| = 8.3 \times 10^{-31} e \text{ cm}$, which is smaller than the current bound by about 1 order of magnitude.

We note in passing that a future measurement of the proton EDM could be another good prober of ρ_{bb} -EWBG. The experimental sensitivity of the proton EDM at IBS-CAPP [53] and BNL [54] is $|d_p| \sim 10^{-29} e \text{ cm}$. As is the case of neutron EDM discussed above, the proton EDM can be estimated by use of the QCD sum rules as [49]

$$d_p = 0.78d_u - 0.20d_d + e(-1.2d_u^C - 0.15d_d^C)/g_3. \quad (42)$$

With this, it is found that $|d_p| = 2.3 \times 10^{-29} e \text{ cm}$ for the parameters used in Fig. 4 with $r = 10^{-3}$. Therefore, the future measurement of d_p could access the ρ_{bb} -EWBG parameter space regardless of the d_e cancellation.

C. Direct search limits

There exist several direct search limits from ATLAS and CMS that may restrict the parameter space of ρ_{bb} , even for $c_\gamma = 0$ and $\rho_{tt} = 0$. The coupling ρ_{bb} receives several constraints from heavy Higgs boson searches at the LHC. In particular, Refs. [55–59] are relevant to our study. We find that the most stringent constraint arises from CMS search involving heavy Higgs boson production in association with at least one b -jet and decaying into $b\bar{b}$ pair based on 13 TeV 35.7 fb $^{-1}$ data [55]. The CMS search provides a model independent 95% CL upper limits on the $\sigma(pp \rightarrow bA/H + X) \cdot \mathcal{B}(A/H \rightarrow b\bar{b})$ in the mass range beginning from 300 GeV to 1300 GeV. We first extract [60] corresponding 95% CL upper limit $\sigma(pp \rightarrow bA/H + X) \cdot \mathcal{B}(A/H \rightarrow b\bar{b})$ for our three BPs. Taking a reference $|\rho_{bb}|$ value, we then estimate the production cross sections of $pp \rightarrow bA/H + X$ at the leading order (LO) utilizing Monte Carlo event generator MadGraph5_aMC@NLO [61] with the default parton distribution function (PDF) NN23LO1 set [62] for the BPs. As the analysis does not veto

additional activity in the event [55], we therefore include contributions from $gg \rightarrow b\bar{b}A/H$ along with $bg \rightarrow bA/H$ while estimating the cross sections. These cross sections are finally rescaled by $|\rho_{bb}|^2 \times \mathcal{B}(A/H \rightarrow b\bar{b})$ to obtain the corresponding 95% CL upper limits on $|\rho_{bb}|$. It is found that $|\rho_{bb}| \gtrsim 0.6$ is excluded for BP*a* at 95% CL and likewise, the regions where $|\rho_{bb}| \gtrsim 0.6$ and $|\rho_{bb}| \gtrsim 0.8$ are ruled out for BP*b* and BP*c*, respectively. These upper limits are rather weak. The limits are even weaker from a similar search performed by ATLAS [56]. We note that while estimating the upper limit on ρ_{bb} we set all $\rho_{ij} = 0$ for simplicity. In general, we remark that non-zero ρ_{ij} would further alleviate these upper limits. Further, ρ_{bb} coupling can induce $pp \rightarrow t(b)H^\pm$ process which is proportional to V_{tb} (see Eq. (7)). These processes are extensively searched by ATLAS [57] and CMS [58, 59] with $H^+/H^- \rightarrow t\bar{b}/\bar{t}b$ decays. We find that the constraints are weaker for all the three BPs, however, as we see below these searches would provide sensitive probe to ρ_{tt} . The effective model is implemented in the FeynRules 2.0 [63] framework.

We now turn to constraints on ρ_{tt} . As ρ_{tt} can also induce V_{tb} , the searches $pp \rightarrow \bar{t}(b)H^+$ followed by $H^+ \rightarrow t\bar{b}$ [57–59] would also be relevant. The ATLAS search [57] is based on $36 \text{ fb}^{-1} \sqrt{s} = 13 \text{ TeV}$ dataset, which provides model independent 95% CL upper limit on $\sigma(pp \rightarrow \bar{t}bH^+) \times \mathcal{B}(H^+ \rightarrow t\bar{b})$ from $m_{H^\pm} = 200 \text{ GeV}$ and 2 TeV . Similar searches are also performed by CMS based on $\sqrt{s} = 13 \text{ TeV}$ 35.9 fb^{-1} dataset [58, 59]. These searches provide 95% CL upper limit on $\sigma(pp \rightarrow \bar{t}H^+) \times \mathcal{B}(H^+ \rightarrow t\bar{b})$ for $m_{H^\pm} = 200 \text{ GeV}$ and 3 TeV in leptonic [58] and, combining leptonic and all-hadronic final states [59]. Like before, the non-vanishing ρ_{tt} enhanced by V_{tb} can induce such process, leading to stringent constraints. To find the constraints, as done before, we calculate the cross sections $\sigma(pp \rightarrow \bar{t}bH^+) \times (H^+ \rightarrow t\bar{b})$ at LO for a reference $|\rho_{tt}|$ for the three BPs via MadGraph5_aMC@NLO. These cross sections are then rescaled by $|\rho_{tt}|^2 \times \mathcal{B}(H^+ \rightarrow t\bar{b})$ to get the corresponding 95% CL upper limits on $|\rho_{tt}|$. The extracted [60] 95% CL upper limits from ATLAS search [57] on ρ_{tt} for the three BPs are $|\rho_{tt}| \gtrsim 1.1, 1.2$ and 1.4 , respectively, while the limits from CMS [59] are much stronger, which read as $|\rho_{tt}| \gtrsim 0.6, 0.7$ and 0.7 , respectively. We remark that the constraints from CMS search with leptonic final state [58] is mildly weaker than the search with combined leptonic and all-hadronic final states [59]. We also note that all the ρ_{ij} except for ρ_{tt} are assumed to be zero when extracting the upper limits for the sake of simplicity. Therefore if other ρ_{ij} are turned on, the limits on ρ_{tt} in general becomes weaker due to dilution from other branching ratios of H^\pm .

The ATLAS [21] and CMS [22] search for heavy Higgs via $gg \rightarrow H/A \rightarrow t\bar{t}$ would also constrain ρ_{tt} . The ATLAS [21] result is based on 20.3 fb^{-1} data at 8 TeV, which provides exclusion limits on $\tan\beta$ vs m_A (or, m_H) in type-II 2HDM framework starting from m_A and $m_H = 500 \text{ GeV}$. The CMS search is based on 35.9 fb^{-1} data at $\sqrt{s} = 13 \text{ TeV}$, which provides upper limit on coupling modifier (see Ref. [22] for definition) the m_A (m_H) from 400 GeV to 750 GeV based on different values of Γ_A/m_A (Γ_H/m_H) ratios. Reinterpreting the ATLAS exclusion limit [21], we find that $|\rho_{tt}| \gtrsim 0.9$ is excluded for BP*a* at 95% CL, whereas $|\rho_{tt}| \gtrsim 0.8$ for BP*b*. There is no upper limit on ρ_{tt} for BP*c* from ATLAS [21] as both m_A and m_H lie beyond the presented $\tan\beta$ - m_A or $\tan\beta$ - m_H . Here, for BP*a*, m_A lies below the search range, therefore the limit is extracted from the observed $\tan\beta$ vs m_H exclusion limit [21]. For BP*a* both m_A and m_H lie within the plotted range of ATLAS search [21] but the observed limit presented in for $\tan\beta$ - m_H stops around $m_A \approx 630 \text{ GeV}$ ATLAS search [21]. On the other hand, from CMS search [22] $|\rho_{tt}|$ is excluded at 95% CL for $|\rho_{tt}| \lesssim 1.1$ (1.3), 0.9 (1.0) and 1.2 (1.4) if $\Gamma_A/m_A = 5\%$ ($\Gamma_A/m_A = 10\%$) for the three BPs respectively. We find that the upper limits from $gg \rightarrow H \rightarrow t\bar{t}$ are always weaker than that of $gg \rightarrow A \rightarrow t\bar{t}$ [22]. We also remark that these upper limits provided by both the collaborations assume that m_A and m_H are decoupled from each other. Although m_A and m_H are separated sufficiently, this is not the case for any of the BPs chosen, as can be seen from Table I. Therefore, the actual upper limits extracted here would be mildly stronger.

Moreover, ρ_{tt} would also receive constraint from CMS search for SM four-top production [64]. The search is performed with 13 TeV 137 fb^{-1} dataset and provides 95% CL upper limits on $\sigma(pp \rightarrow t\bar{t}A/t\bar{t}H) \times \mathcal{B}(A/H \rightarrow t\bar{t})$ for $350 \text{ GeV} \leq m_{A/H} \leq 650 \text{ GeV}$. The search also includes contributions from $\sigma(pp \rightarrow tWA/H, tqA/H)$ followed by $A/H \rightarrow t\bar{t}$, which can also be induced by ρ_{tt} . To understand how strong the constraints could be, we generate these cross sections at LO by MadGraph5_aMC@NLO for a reference value of $|\rho_{tt}|$ setting all other $\rho_{ij} = 0$, and then rescale simply by $|\rho_{tt}|^2 \times \mathcal{B}(A/H \rightarrow t\bar{t})$. It is found that $|\rho_{tt}| \gtrsim 1.0$, 1.1 and 1.3 for the three BPs at 95% CL, respectively. As in the case of $gg \rightarrow H/A \rightarrow t\bar{t}$, the search here also assumes that m_A and m_H are decoupled from each other. Therefore, one expects the limits to be mildly stronger for all the three BPs.

We finally conclude that $|\text{Im}(\rho_{bb})| \sim 0.15$ and $\rho_{tt} \sim 0.5$ are well allowed by the current measurements for the mass spectrum under consideration. We take these values as repre-

BP	$\mathcal{B}(A \rightarrow t\bar{t})$	$\mathcal{B}(A \rightarrow b\bar{b})$
a	0.86	0.14
b	0.89	0.11
c	0.90	0.10

TABLE II. Branching ratios of A for the benchmark points with $\text{Re}(\rho_{bb}) = 0.0$, $\text{Im}(\rho_{bb}) = 0.15$ and $\rho_{tt} = 0.5$.

sentative values for our analysis with $\text{Re}(\rho_{bb}) = 0$.⁴ Under the assumptions, i.e., setting all $\rho_{ij} = 0$ except ρ_{bb} and ρ_{tt} , the total decay width of A can be nicely approximated as the sum of the partial widths of $A \rightarrow t\bar{t}$ and $A \rightarrow b\bar{b}$ decays for all the three BPs. The total decay widths of A are 3.94 GeV, 6.43 GeV and 7.84 GeV respectively for the three BPs with $|\text{Im}(\rho_{bb})| \sim 0.15$ and $\rho_{tt} \sim 0.5$. The corresponding branching ratios are presented in Table II. Note that when calculating decay widths and branching ratios of A , we neglect tiny loop induced decays such as $A \rightarrow \gamma\gamma$, $A \rightarrow Z\gamma$ etc.

IV. COLLIDER SIGNATURE

Having found the parameter space for ρ_{bb} and ρ_{tt} , we now discuss the discovery potential of $pp \rightarrow bA + X \rightarrow bt\bar{t} + X$, followed by semileptonic decay of at least one top quark, constituting three b -jets, at least one charged lepton (e and μ) and missing transverse energy (E_T^{miss}) signature, which we denote as $3b1\ell$ process. Note that such final state receives mild contributions from $pp \rightarrow bH + X \rightarrow bt\bar{t} + X$ process which is included in our analysis. Further, $bg \rightarrow \bar{t}H^+ \rightarrow \bar{t}t\bar{b}$ process may also contribute to the same final state topologies, if at least one of the top decays semileptonically. However, it turns out that such contributions are even milder for all the three BPs so that we neglect them in our analysis.

There exist several SM backgrounds. The dominant backgrounds are $t\bar{t}$ +jets, t - and s -channel single-top (tj), Wt , with subdominant backgrounds from $t\bar{t}h$ and, $t\bar{t}Z$ productions. Further, small contributions come from Drell-Yan+jets, W +jets, four-top ($4t$), $t\bar{t}W$, tW h, which are collectively denoted as ‘‘Others’’. We do not include backgrounds originating from

⁴ As discussed before, both ρ_{bb} and ρ_{tt} can induce $pp \rightarrow t(b)H^\pm$ process, hence, the constraints from Ref. [59] would become stronger if both the couplings are non-vanishing. However, we have checked that $\rho_{tt} \sim 0.5$ is allowed for $|\text{Im}(\rho_{bb})| \sim 0.15$ for all the three BPs.

non-prompt and fake sources. These backgrounds are not properly modeled in Monte Carlo event generators and one requires data to estimate such contributions.

The signal and background event samples are generated in pp collision at $\sqrt{s} = 14$ TeV CM energy at LO by MadGraph5_aMC@NLO with NN23LO1 PDF set as done before and then interfaced with Pythia 6.4 [65] for hadronization and showering and finally fed into Delphes 3.4.2 [66] for fast detector simulation adopting default ATLAS-based detector card of Delphes. We adopt MLM scheme [67, 68] for matrix element and parton shower merging.

The LO $t\bar{t}$ +jets background cross section is normalized up to the NNLO (next-to-next-to LO) by a factor of 1.84 [69] while t - and s -channel single-top cross sections are normalized by factors of 1.2 and 1.47, respectively [70]. The LO Wt +jets background is normalized to the NLO cross section by a factor of 1.35 [71], whereas the subdominant $t\bar{t}h$ and $t\bar{t}Z$ are corrected to corresponding NLO ones by factors of 1.27 [72] and 1.56 [73] respectively. The DY+jets background is normalized to NNLO cross sections by factor of 1.27 [74, 75]. Finally, the LO cross sections $4t$ and $t\bar{t}W$ are adjusted to the NLO ones by factors of 2.04 [61] and 1.35 [76], respectively. The tWh and W +jets background are kept at LO. For simplicity we assume the correction factors for the charge conjugate processes to be the same. We remark that the signal cross sections for all the three BPs are kept at LO.

The events are selected in a way such that they should contain at least one charged lepton (e and μ), at least three b -tagged and some E_T^{miss} . The normalized transverse momentum (p_T) distributions of the leading and subleading b -jets for the signal and leading backgrounds

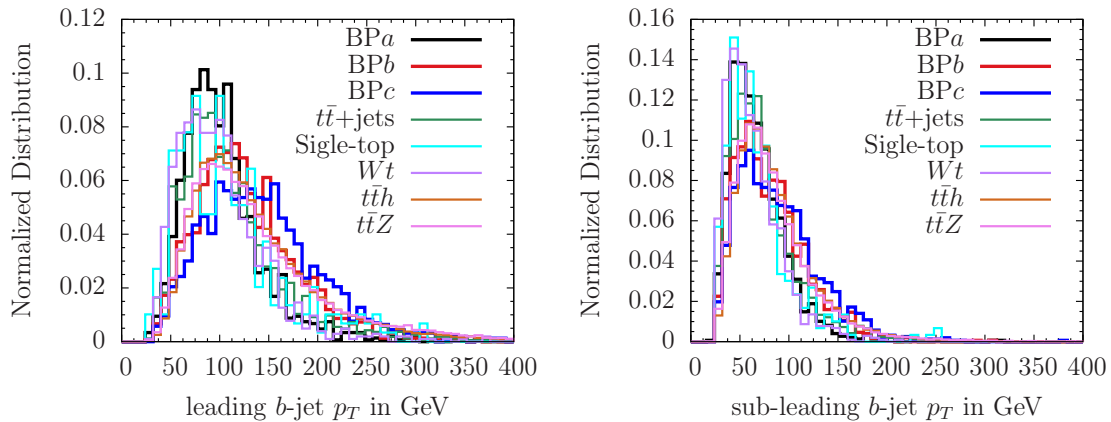


FIG. 5. The normalized p_T distributions of the leading and subleading b -jets for the signal and the leading backgrounds.

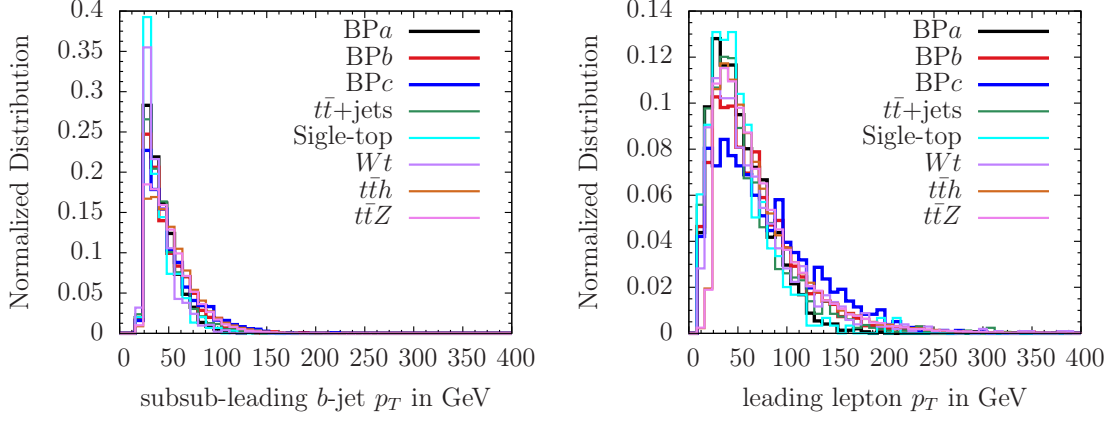


FIG. 6. The normalized p_T distributions of the subsubleading b -jet (right) and leading lepton (left) for the signal and leading backgrounds.

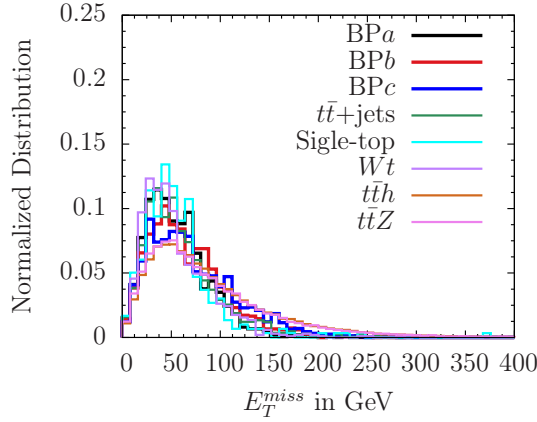


FIG. 7. The normalized missing energy E_T^{miss} (right) for the signal and leading backgrounds.

are presented in Fig 5. The p_T distributions for the subsubleading b -jet and leading lepton are plotted in Fig 6, while the normalized E_T^{miss} distributions are shown in Fig 7. To reduce backgrounds we apply the following event selection cuts. p_T of all three b -jets should be $p_T > 20$ GeV, whereas that of the leading lepton should be $p_T > 25$ GeV. The absolute value of pseudo-rapidity ($|\eta|$) of all three b -jets and lepton should be less than 2.5. The minimum separation (ΔR) between the lepton and any b -jet as well as that between any two b -jets are required to be greater than 0.4. E_T^{miss} in each event should be larger than 35 GeV. The jets are reconstructed by anti- k_t algorithm using a radius parameter $R = 0.6$. We adopt default b -jet tagging and light jets rejection efficiencies of Delphes ATLAS based detector card. Note that in our exploratory study we do not optimize the selection cuts such as p_T , η or E_T^{miss}

and keep them unchanged for all the BPs for simplicity. The total background cross sections along with different components after the selection cuts are shown in Table III, whereas the signal cross sections for the BPs and corresponding statistical significances for 600 (3000) fb^{-1} integrated luminosity are summarized in Table. IV. The statistical significances in Table IV are estimated using $\mathcal{Z} = \sqrt{2[(S+B)\ln(1+S/B) - S]}$ [77], where S and B are the numbers of the signal and background events.

$t\bar{t} + \text{jets}$	Single-top	$Wt + \text{jets}$	$t\bar{t}h$	$t\bar{t}Z$	Others	Total Bkg. (fb)
3953.49	98.93	77.93	10.72	4.13	30.85	4176.05

TABLE III. The cross sections (in units of fb) of the different background components for $3b1\ell$ process after selection cuts at $\sqrt{s} = 14$ TeV.

BP	Signal (fb)	Significance (\mathcal{Z}) 600 (3000) fb^{-1}
a	11.11	4.2 (9.4)
b	5.94	2.2 (5.0)
c	3.86	1.5 (3.3)

TABLE IV. The cross sections of the $3b1\ell$ process for the different BPs assuming $\text{Im}(\rho_{bb}) = 0.15$ and $\rho_{tt} = 0.5$. The corresponding significances with 600 (3000) fb^{-1} integrated luminosities of the three BPs are given in third column.

Let us discuss the achievable significances for the $3b1\ell$ process as summarized in Table IV. The significance of the BP a , BP b and BP c are $\sim 4.2\sigma$, $\sim 2.2\sigma$ and $\sim 1.5\sigma$ with 600 fb^{-1} integrated luminosity. The significances can reach up to $\sim 9.4\sigma$, $\sim 5\sigma$ and $\sim 3.3\sigma$ respectively with the full HL-LHC dataset (3000 fb^{-1} integrated luminosity). We find that for BP a evidence ($\sim 3\sigma$) might be possible in the Run-3 of LHC, while $\sim 2\sigma$ significance is possible with the collected Run-2 data (137 fb^{-1}). Rescaling these numbers, we find that one may discover the process if $360 \lesssim m_A \lesssim 520$ GeV, whereas strong evidence might

emerge in the Run-3 data if $m_A \sim 400$ GeV. We also find that if $|\text{Im}(\rho_{bb})| = 0.07$, which is mildly larger than the nominal $|\text{Im}(\rho_{bb})| = 0.058$ required for successful ρ_{bb} -EWBG [10], one has $\sim 2.3\sigma$ significance for BP*a* with the HL-LHC dataset. By a simple rescaling, we also find that for BP*b* and BP*c* the constraints on $|\text{Im}(\rho_{bb})|$ with the HL-LHC dataset would be relatively milder. It is remarked that we always take $\rho_{tt} = 0.5$ in the scalings. We also remark that our chosen values $|\text{Im}(\rho_{bb})| = 0.15$ and $\rho_{tt} = 0.5$ are only for illustration and we have not saturated these couplings to the corresponding upper limits. Therefore the achievable significances summarized in Table IV in general can be enhanced further for all three BPs.

Before closing, we discuss the impact of the other ρ_{ij} couplings. So far, we have set all $\rho_{ij} = 0$ except ρ_{bb} and ρ_{tt} . Presence of the other ρ_{ij} couplings open up other decay modes of A , which in principle may reduce the achievable significances summarized in Table IV. For instance, if $\rho_{\tau\tau} \sim \lambda_\tau$, it would induce $A \rightarrow \tau^+\tau^-$ decay. However, the significances remain practically same for all the three BPs. Moreover, $\rho_{tc} \sim 0.4\text{--}0.5$ would induce $cg \rightarrow tA/tH \rightarrow tt\bar{c}$ (same-sign top) [15, 78] (see also Refs. [79–81]) and $cg \rightarrow tA/tH \rightarrow tt\bar{c}$ (triple-top) signature, which might emerge in the Run-3 of LHC.

V. THE $gg \rightarrow t\bar{t}A \rightarrow t\bar{t}b\bar{b}$ PROCESS

We now briefly discuss the discovery potential of $gg \rightarrow t\bar{t}A \rightarrow t\bar{t}b\bar{b}$ process. The process can in principle probe the parameter space for ρ_{bb} -EWBG mechanism if $m_A < 2m_t$. We search this process via $pp \rightarrow t\bar{t}A + X \rightarrow t\bar{t}b\bar{b} + X$, followed by at least one top quark decaying semileptonically i.e., with four b -jets, at least one charged lepton and E_T^{miss} signature. The final state topology receives mild contributions from inclusive $pp \rightarrow WtA + X$ and $pp \rightarrow tjA + X$ processes. As we show below, the signature is not promising as opposed to $bg \rightarrow bA \rightarrow bt\bar{t}$ process.

To understand the discovery potential, we first choose a benchmark point in which $m_A < 2m_t$. In particular, we take $m_A = 318$ GeV, $m_{H^\pm} = 426$ GeV, $m_H = 495$ GeV, $\eta_1 = 0.258$, $\eta_2 = 1.5$, $\eta_3 = 2.934$, $\eta_4 = -0.285$, $\eta_5 = 2.378$, $\eta_6 = 0$, $\eta_7 = 0.751$ and $\mu_{22}^2/v^2 = 1.52$ which satisfy perturbativity, tree-level unitarity and vacuum stability conditions as well as the oblique T parameter constraint. The parameter space for ρ_{tt} and ρ_{bb} would receive similar constraints as in Sec. III. We find that $|\rho_{tt}| = 0.5$ and $|\rho_{bb}| = 0.1$ are still allowed by the

current data. Under these assumptions $\mathcal{B}(A \rightarrow b\bar{b})$ is practically $\approx 100\%$ and the total decay width of A is 0.19 GeV.

We generate events at LO as in $3b1\ell$ process, i.e., via MadGraph5_aMC@NLO followed by hadronization and showering in Pythia and finally incorporate the detector effects of Delphes ATLAS based detector card. The dominant backgrounds arise from the $t\bar{t}+$ jets, Single-top and $Wt+$ jets, whereas $t\bar{t}h$, $t\bar{t}Z$ and $4t$ constitute subdominant backgrounds. We assume the same QCD corrections factor as in $3b1\ell$ process for simplicity.

Signal	$t\bar{t}+$ jets	Single-top	$Wt+$ jets	Others	Total Bkg. (fb)
0.19	197.28	1.13	1.39	3.21	203.02

TABLE V. The cross sections (in units of fb) of signal and the different background components for $4b1\ell$ process after selection cuts at $\sqrt{s} = 14$ TeV.

To reduce the background, we use the following event selection cuts. The events are selected so that they contain at least one lepton (e and μ), at least four jets with at least four are b -tagged and some missing E_T^{miss} (denoted as $4b1\ell$ process). The lepton is required to have $p_T > 25$ GeV and $|\eta| < 2.5$. For any jet in the event $p_T > 20$ GeV and $|\eta| < 2.5$. E_T^{miss} in each event is required to be greater than 35 GeV. The separation ΔR between any two jets as well as that between a jet and a lepton should be larger than 0.4. Finally, we construct all possible combinations of the invariant mass m_{jj} from the four leading jets and demand that the one closest to m_A should lie between $|m_A - m_{jj}| < 40$ GeV. The impact of these cuts on the signal and background processes are summarized in Table V.

We find that the achievable significance of the $gg \rightarrow t\bar{t}A \rightarrow t\bar{t}b\bar{b}$ process is $\sim 1\sigma$ with 3000 fb^{-1} integrated luminosity, which is rather low. This means that no meaningful constraints can be extracted unless both ATLAS and CMS data are added. It should be remarked that since we use the same QCD correction factors for the backgrounds as in $bg \rightarrow bA \rightarrow b\bar{t}\bar{t}$ process, there are greater uncertainties in these cross sections.

VI. DISCUSSION AND SUMMARY

Motivated by electroweak baryogenesis induced by the extra bottom Yukawa coupling ρ_{bb} we have analyzed the discovery prospect of $pp \rightarrow bA + X \rightarrow bt\bar{t} + X$ process. We searched the $pp \rightarrow bA + X \rightarrow bt\bar{t} + X$ process where at least one top decays semileptonically, comprising with three b -tagged jets, at least one charged lepton and E_T^{miss} signature at the 14 TeV LHC. We chose three benchmark points for m_A ranging from 400 GeV to 600 GeV for illustration and took moderately large $|\rho_{bb}| \sim 0.15$ while ρ_{tt} is set to ~ 0.5 . We find that the statistical significance for the three BPs can reach up to $\sim 9.4\sigma$, $\sim 5\sigma$ and $\sim 3.3\sigma$ respectively with the full HL-LHC dataset, while $\sim 4.2\sigma$, $\sim 2.2\sigma$ and, $\sim 1.5\sigma$ significances with 600 fb $^{-1}$ dataset. For BP*a*, where $m_A \sim 400$ GeV, evidence ($\sim 3\sigma$) may emerge in the Run-3 data, while $\sim 2\sigma$ significance might be already in the awaiting in the collected Run-2 data (137 fb $^{-1}$). We found that for BP*a*, $pp \rightarrow bA + X \rightarrow bt\bar{t} + X$ process can probe $|\text{Im}(\rho_{bb})| \sim 0.07$ at the HL-LHC if $\rho_{tt} \sim 0.5$. This is slightly above the nominal $|\text{Im}(\rho_{bb})| \gtrsim 0.058$ required for the successful ρ_{bb} -EWBG mechanism. This means that $bg \rightarrow bA \rightarrow bt\bar{t}$ process can probe most of the parameter space for ρ_{bb} -EWBG if $m_A \sim 400$ GeV. We also remark that the constraints on ρ_{tt} would also evolve simultaneously and improve as the data collection goes on at the LHC [82]. This would allow one to probe even larger part of the parameter space.

Discovery is possible via $pp \rightarrow bA + X \rightarrow bt\bar{t} + X$ process, however, to attribute the discovery to ρ_{bb} -EWBG mechanism is beyond the scope of LHC as information of the CP-violating phase of ρ_{bb} is lost in pp collision. In this regard, $\Delta\mathcal{A}_{\text{CP}}$ of $\mathcal{B}(B \rightarrow X_s\gamma)$ would provide very sensitive probe for the $\text{Im}(\rho_{bb})$ even though the observable has uncertainties associated with the hadronic parameter $\tilde{\Lambda}_{78}$. While finding the constraints in Fig. 2, we assumed $\tilde{\Lambda}_{78} = 89$ MeV, which is the average of $17 \text{ MeV} \leq \tilde{\Lambda}_{78} \leq 190 \text{ MeV}$ [41]. However, if $\tilde{\Lambda}_{78}$ is taken as its upper range, the constraint becomes much severe for $\text{Im}(\rho_{bb})$. Furthermore, on the experimental side, projected Belle II accuracy of $\Delta\mathcal{A}_{\text{CP}}$ measurement is $\sim 5\%$ [83]. Therefore, more precise estimation of $\tilde{\Lambda}_{78}$ together with Belle II measurement can stringently probe the parameter space of $\text{Im}(\rho_{bb})$ unless the CP-violating phases of ρ_{tt} and ρ_{bb} are aligned [11] in which $\Delta\mathcal{A}_{\text{CP}} = 0$. In such a case, measurements of EDMs play a pivotal role in probing $\text{Im}(\rho_{bb})$.

The unprecedented electron EDM constraint set by ACME Collaboration in 2008 reduces most EWBG scenarios to despair. We updated our previous analysis done in Ref. [10]

including all the relevant Barr-Zee diagrams. Because of the significant contributions arising from the diagrams involving ρ_{ee} , the cancellation mechanism can be effective. It was found that the electron EDM cancellation in ρ_{bb} -EWBG belongs to the unstructured cancellation category in which the diagonal hierarchical structures of ρ_{ij}^F are much different from those of the SM Yukawa couplings, which is in stark contrast to the case in ρ_{tt} -EWBG that can accommodate the structured cancellation [11]. Nonetheless, the viable parameter space of ρ_{bb} -EWBG still exists. Besides the extreme fine tuning of the parameters, ρ_{bb} -EWBG would be confirmed or ruled out if the electron EDM is improved down to $\sim 10^{-30}$ e cm level. Moreover, as discussed in Sec. III B, the future measurement of the proton EDM could play a complementary role in probing ρ_{bb} -EWBG.

In principle $pp \rightarrow bA + X \rightarrow bt\bar{t} + X$ process can also be induced by ρ_{bd} , ρ_{db} , ρ_{bs} and ρ_{sb} at the LHC. However, due to severe constraints arising from B_d and B_s mixings [84] their impacts typically are inconsequential. In addition if the charm quark gets misidentified as b -jet, a sizable ρ_{cc} can also mimic similar signature in pp collision via $cg \rightarrow cA \rightarrow ct\bar{t}$ process. We remark that such possibilities can be disentangled by the simultaneous application of b - and c -tagging on the final state topologies [85].

So far we have not discussed the uncertainties. As a first estimate, uncertainties arising from factorization scale (μ_F) and renormalization scale (μ_R) dependences are not included in our LO cross section estimations. In general, the LO $bg \rightarrow bA/bH$ processes have $\sim 25 - 30\%$ scale uncertainties for $m_{A/H} \sim (300 - 400)$ GeV if bottom quark with $p_T > (15 - 30)$ GeV and, $|\eta| < 2.5$ [86] (see also [87–89]). It has been found that [90] the LO cross sections calculated with LO PDF set CTEQ6L1 [91] have relatively higher factorization scale dependence. Therefore, we remark that the LO cross sections in our analysis, which we estimated with LO NN23LO1 PDF set, might have same level of uncertainties. It has also been found that [90] for $\mu_F \approx m_A$ (or m_H) the corrections to the LO cross sections could be large negative ($\sim -70\%$), whereas for the choice of $\mu_F \approx m_A/4$ (or $m_H/4$) the corrections are mild; which indicates that the $\mu_F \approx m_A/4$ is the relevant factorization scale. Furthermore, the cross section uncertainties from factorization scale and renormalization choices are found to be particularly small at $\mu_R = m_A$ and if varied from $\mu_R = m_A/2$ to $\mu_R = 2m_A$, along with $\mu_F = m_A/4$ and varied from $\mu_F = m_A/8$ to $\mu_F = m_A/2$ [90]. In addition, our analysis does not include PDF uncertainties, which could be in general significant for any bottom-quark initiated process as discussed, e.g., in Ref. [92]. Detailed

discussions on different PDFs and associated uncertainties for the LHC are summarized in Ref. [93]. These typically would induce some uncertainties in our results. We leave out the detailed estimation of these uncertainties for future work.

In summary, motivated by electroweak baryogenesis induced by extra bottom Yukawa coupling ρ_{bb} we have explored the possibility of discovering $bg \rightarrow bA \rightarrow bt\bar{t}$ process at the 14 TeV LHC. We find that the process can be discovered for $360 \text{ GeV} \lesssim m_A \lesssim 520 \text{ GeV}$. While LHC can indeed discover the process, however, the information of the CP-violating phase of ρ_{bb} can only be probed via $\Delta\mathcal{A}_{\text{CP}}$ of $\mathcal{B}(B \rightarrow X_s\gamma)$ or the EDM measurements of the electron, neutron and mercury though the latter two have the less probing power to date. For completeness we also studied $gg \rightarrow t\bar{t}A \rightarrow t\bar{t}b\bar{b}$ process and found that it is not promising. In conclusion, together with the electron EDM measurement and/or $\Delta\mathcal{A}_{\text{CP}}$ of $\mathcal{B}(B \rightarrow X_s\gamma)$ decay, the discovery of $bg \rightarrow bA \rightarrow bt\bar{t}$ process may help us to understand the mechanism behind the observed matter-antimatter asymmetry of the Universe.

Acknowledgments.— TM thanks Osaka University and Prof. Shiniya Kanemura for affiliation. TM was supposed to join Osaka University as a postdoctoral fellow in April but delayed due to travel restrictions related to ongoing pandemic. TM also thanks National Taiwan University and Prof. Wei-Shu Hou for temporary visiting position.

Appendix A: EDMs

For the EDM calculations, the following parametrization is also useful.

$$\mathcal{L}_{\phi\bar{f}f} = -\phi\bar{f}(g_{\phi\bar{f}f}^S + i\gamma_5 g_{\phi\bar{f}f}^P)f, \quad (\text{A1})$$

where $\phi = h, H, A$ and

$$g_{h\bar{f}f}^S = \frac{1}{\sqrt{2}}[\lambda_f s_\gamma + \text{Re}\rho_{ff}c_\gamma], \quad g_{h\bar{f}f}^P = \frac{1}{\sqrt{2}}\text{Im}\rho_{ff}c_\gamma, \quad (\text{A2})$$

$$g_{H\bar{f}f}^S = \frac{1}{\sqrt{2}}[\lambda_f c_\gamma - \text{Re}\rho_{ff}s_\gamma], \quad g_{H\bar{f}f}^P = -\frac{1}{\sqrt{2}}\text{Im}\rho_{ff}s_\gamma, \quad (\text{A3})$$

$$g_{A\bar{f}f}^S = \pm\frac{1}{\sqrt{2}}\text{Im}\rho_{ff}, \quad g_{A\bar{f}f}^P = \mp\frac{1}{\sqrt{2}}\text{Re}\rho_{ff}, \quad (\text{A4})$$

where the upper sign is for up-type fermions and the lower for down-type fermions in Eq. (A4).

Here we list the loop functions appearing in the EDM calculations in Sec. III B.

$$f(\tau) = \frac{\tau}{2} \int_0^1 dx \frac{1 - 2x(1-x)}{x(1-x) - \tau} \ln \left(\frac{x(1-x)}{\tau} \right), \quad (\text{A5})$$

$$g(\tau) = \frac{\tau}{2} \int_0^1 dx \frac{1}{x(1-x) - \tau} \ln \left(\frac{x(1-x)}{\tau} \right), \quad (\text{A6})$$

$$\begin{aligned} \mathcal{J}_W^V(m_\phi) = & \frac{2m_W^2}{m_\phi^2 - m_V^2} \left[-\frac{1}{4} \left\{ \left(6 - \frac{m_V^2}{m_W^2} \right) + \left(1 - \frac{m_V^2}{2m_W^2} \right) \frac{m_\phi^2}{m_W^2} \right\} \right. \\ & \times (I_1(m_W, m_\phi) - I_1(m_W, m_V)) \\ & + \left\{ \left(-4 + \frac{m_V^2}{m_W^2} \right) + \frac{1}{4} \left(6 - \frac{m_V^2}{m_W^2} \right) + \frac{1}{4} \left(1 - \frac{m_V^2}{2m_W^2} \right) \frac{m_\phi^2}{m_W^2} \right\} \\ & \left. \times (I_2(m_W, m_\phi) - I_2(m_W, m_V)) \right], \quad (\text{A7}) \end{aligned}$$

$$J_1(\tau_{WH^\pm}, \tau_{tH^\pm}) = \int_0^1 \frac{dx}{x} (2-x) \left[Q_t(1-x) J \left(\tau_{WH^\pm}, \frac{\tau_{tH^\pm}}{x} \right) + Q_b x J \left(\tau_{WH^\pm}, \frac{\tau_{tH^\pm}}{x} \right) \right], \quad (\text{A8})$$

where $\tau_{ij} = m_i^2/m_j^2$, $Q_t = 2/3$, $Q_b = -1/3$ and

$$I_1(m_1, m_2) = -2 \frac{m_2^2}{m_1^2} f \left(\frac{m_1^2}{m_2^2} \right), \quad I_2(m_1, m_2) = -2 \frac{m_2^2}{m_1^2} g \left(\frac{m_1^2}{m_2^2} \right), \quad (\text{A9})$$

$$J(a, b) = \frac{1}{a-b} \left[\frac{a}{a-1} \ln a - \frac{b}{b-1} \ln b \right]. \quad (\text{A10})$$

-
- [1] M. Tanabashi *et al.* [Particle Data Group], Phys. Rev. D **98**, 030001 (2018).
[2] A.D. Sakharov, Pisma Zh. Eksp. Teor. Fiz. **5**, 32 (1967).
[3] G. Aad *et al.* [ATLAS Collaboration], Phys. Lett. B **716**, 1 (2012); S. Chatrchyan *et al.* [CMS Collaboration], *ibid.* B **716**, 30 (2012).
[4] V.A. Kuzmin, V.A. Rubakov and M.E. Shaposhnikov, Phys. Lett. B **155**, 36 (1985). For some reviews, see e.g. M. Quiros, Helv. Phys. Acta **67**, 451 (1994); V.A. Rubakov and M.E. Shaposhnikov, Usp. Fiz. Nauk **166**, 493 (1996) [Phys. Usp. **39**, 461 (1996)]; K. Funakubo, Prog. Theor. Phys. **96**, 475 (1996); A. Riotto, [arXiv:hep-ph/9807454 [hep-ph]]; M. Trodden, “Electroweak baryogenesis,” Rev. Mod. Phys. **71**, 1463 (1999); W. Bernreuther, Lect. Notes Phys. **591**, 237 (2002); J.M. Cline, arXiv:hep-ph/0609145; D.E. Morrissey and M.J. Ramsey-Musolf, New J. Phys. **14**, 125003 (2012); T. Konstandin, Phys. Usp. **56**, 747 (2013); E. Senaha, Symmetry **12** (2020) no.5, 733.

- [5] A. Bochkarev, S. Kuzmin and M. Shaposhnikov, Phys. Lett. B **244** (1990), 275-278; K. Funakubo, A. Kakuto and K. Takenaga, Prog. Theor. Phys. **91** (1994), 341-352; J. M. Cline and P. A. Lemieux, Phys. Rev. D **55** (1997), 3873-3881; S. Kanemura, Y. Okada and E. Senaha, Phys. Lett. B **606**, 361 (2005); L. Fromme, S. J. Huber and M. Seniuch, JHEP **11** (2006), 038; T. A. Chowdhury, M. Nemevsek, G. Senjanovic and Y. Zhang, JCAP **02** (2012), 029; D. Borah and J. M. Cline, Phys. Rev. D **86** (2012), 055001; J. M. Cline and K. Kainulainen, Phys. Rev. D **87** (2013) no.7, 071701; G. Gil, P. Chankowski and M. Krawczyk, Phys. Lett. B **717** (2012), 396-402; G. Dorsch, S. Huber and J. No, JHEP **10** (2013), 029; G. Dorsch, S. Huber, K. Mimasu and J. No, Phys. Rev. Lett. **113** (2014) no.21, 211802; N. Blinov, S. Profumo and T. Stefaniak, JCAP **07** (2015), 028; K. Fuyuto and E. Senaha, Phys. Lett. B **747** (2015), 152-157; P. Basler, M. Mhlleitner and J. Wittbrodt, JHEP **03** (2018), 061; K. Kainulainen, V. Keus, L. Niemi, K. Rummukainen, T. V. Tenkanen and V. Vaskonen, JHEP **06** (2019), 075; F. P. Huang and E. Senaha, Phys. Rev. D **100** (2019) no.3, 035014; X. Wang, F. P. Huang and X. Zhang, Phys. Rev. D **101** (2020) no.1, 015015.
- [6] M. Pietroni, Nucl. Phys. B **402** (1993), 27-45; J. Espinosa, M. Quiros and F. Zwirner, Phys. Lett. B **307** (1993), 106-115; A. Brignole, J. Espinosa, M. Quiros and F. Zwirner, Phys. Lett. B **324** (1994), 181-191; A. Davies, C. Froggatt and R. Moorhouse, Phys. Lett. B **372** (1996), 88-94; J. Espinosa, Nucl. Phys. B **475** (1996), 273-292; B. de Carlos and J. Espinosa, Nucl. Phys. B **503** (1997), 24-54; S. Huber and M. Schmidt, Nucl. Phys. B **606** (2001), 183-230; K. Funakubo, S. Tao and F. Toyoda, Prog. Theor. Phys. **109** (2003), 415-432; K. Funakubo, S. Tao and F. Toyoda, Prog. Theor. Phys. **114** (2005), 369-389; S. J. Huber, T. Konstandin, T. Prokopec and M. G. Schmidt, Nucl. Phys. B **757** (2006), 172-196; K. Funakubo and E. Senaha, Phys. Rev. D **79** (2009), 115024; C. W. Chiang and E. Senaha, JHEP **06** (2010), 030; D. J. Chung and A. J. Long, Phys. Rev. D **81** (2010), 123531; S. Kanemura, E. Senaha and T. Shindou, Phys. Lett. B **706** (2011), 40-45; M. Carena, N. R. Shah and C. E. Wagner, Phys. Rev. D **85** (2012), 036003; R. Fok, G. D. Kribs, A. Martin and Y. Tsai, Phys. Rev. D **87** (2013) no.5, 055018; S. Kanemura, E. Senaha, T. Shindou and T. Yamada, JHEP **05** (2013), 066; J. Kozaczuk, S. Profumo, L. S. Haskins and C. L. Wainwright, JHEP **01** (2015), 144; P. Athron, C. Balazs, A. Fowlie, G. Pozzo, G. White and Y. Zhang, JHEP **11** (2019), 151.
- [7] J. Choi and R. Volkas, Phys. Lett. B **317** (1993), 385-391; S. Ham, Y. Jeong and S. Oh,

- J. Phys. G **31** (2005) no.8, 857-871; A. Ahriche, Phys. Rev. D **75** (2007), 083522; S. Profumo, M. J. Ramsey-Musolf and G. Shaughnessy, JHEP **08** (2007), 010; J. R. Espinosa and M. Quiros, Phys. Rev. D **76** (2007), 076004; A. Ashoorioon and T. Konstandin, JHEP **07** (2009), 086; D. J. Chung and A. J. Long, Phys. Rev. D **84** (2011), 103513; J. R. Espinosa, T. Konstandin and F. Riva, Nucl. Phys. B **854** (2012), 592-630; J. R. Espinosa, B. Gripaios, T. Konstandin and F. Riva, JCAP **01** (2012), 012; J. M. Cline and K. Kainulainen, JCAP **01** (2013), 012; J. M. Cline, K. Kainulainen, P. Scott and C. Weniger, Phys. Rev. D **88** (2013), 055025; K. Fuyuto and E. Senaha, Phys. Rev. D **90** (2014) no.1, 015015; T. Alanne, K. Tuominen and V. Vaskonen, Nucl. Phys. B **889** (2014), 692-711; S. Profumo, M. J. Ramsey-Musolf, C. L. Wainwright and P. Winslow, Phys. Rev. D **91** (2015) no.3, 035018; D. Curtin, P. Meade and C. T. Yu, JHEP **11** (2014), 127; J. Kozaczuk, JHEP **10** (2015), 135; V. Vaskonen, Phys. Rev. D **95** (2017) no.12, 123515; D. Curtin, P. Meade and H. Ramani, Eur. Phys. J. C **78** (2018) no.9, 787; G. Kurup and M. Perelstein, Phys. Rev. D **96** (2017) no.1, 015036; C. W. Chiang, M. J. Ramsey-Musolf and E. Senaha, Phys. Rev. D **97** (2018) no.1, 015005; F. P. Huang, Z. Qian and M. Zhang, Phys. Rev. D **98** (2018) no.1, 015014; C. W. Chiang, Y. T. Li and E. Senaha, Phys. Lett. B **789** (2019), 154-159; A. Beniwal, M. Lewicki, M. White and A. G. Williams, JHEP **02** (2019), 183.
- [8] S. Tulin and P. Winslow, Phys. Rev. D **84** (2011) 034013; J. M. Cline, K. Kainulainen and M. Trott, JHEP **1111** (2011) 089; T. Liu, M. J. Ramsey-Musolf and J. Shu, Phys. Rev. Lett. **108** (2012) 221301; C. Chiang, K. Fuyuto and E. Senaha, Phys. Lett. B **762** (2016), 315-320; H. K. Guo, Y. Y. Li, T. Liu, M. Ramsey-Musolf and J. Shu, Phys. Rev. D **96** (2017) no.11, 115034.
- [9] K. Fuyuto, W.-S. Hou, E. Senaha, Phys. Lett. B **776**, 402 (2018).
- [10] T. Modak and E. Senaha, Phys. Rev. D **99**, 115022 (2019).
- [11] K. Fuyuto, W. Hou and E. Senaha, Phys. Rev. D **101**, 011901 (2020).
- [12] K. Ishikawa, T. Kitahara and M. Takimoto, Phys. Rev. D **91**, 055004 (2015); I. Baldes and G. Servant, JHEP **10**, 053 (2018); O. Matsedonskyi and G. Servant, [arXiv:2002.05174 [hep-ph]].
- [13] For pedagogical reviews on 2HDM see e.g.; A. Djouadi, Phys. Rept. **457**, 1 (2008). G.C. Branco, P.M. Ferreira, L. Lavoura, M.N. Rebelo, M. Sher and J.P. Silva, Phys. Rept. **516**, 1 (2012); and references there in.

- [14] N. Cabibbo, Phys. Rev. Lett. **10**, 531 (1963);
- [15] M. Kohda, T. Modak and W. S. Hou, Phys. Lett. B **776**, 379 (2018).
- [16] T. Modak, Phys. Rev. D **100**, 035018 (2019).
- [17] See, e.g., S. Davidson and H.E. Haber, Phys. Rev. D **72**, 035004 (2005).
- [18] W.-S. Hou, M. Kikuchi, EPL **123**, 11001 (2018).
- [19] S. Gori, I. W. Kim, N. R. Shah and K. M. Zurek, Phys. Rev. D **93**, 075038 (2016);
- [20] For recent discussions see e.g., A. Djouadi, L. Maiani, A. Polosa, J. Quevillon and V. Riquer, JHEP **1506**, 168 (2015); N. Craig, F. D'Eramo, P. Draper, S. Thomas and H. Zhang, JHEP **1506**, 137 (2015); J. Hajer, Y. Y. Li, T. Liu and J. F. H. Shiu, JHEP **1511**, 124 (2015); E. Alvarez and M. Estevez, Phys. Rev. D **96**, 035016 (2017).
- [21] M. Aaboud *et al.* [ATLAS Collaboration], Phys. Rev. Lett. **119**, 191803 (2017).
- [22] A.M. Sirunyan *et al.* [CMS Collaboration], arXiv:1908.01115 [hep-ex].
- [23] For a recent reference, see M. Carena and Z. Liu, JHEP **1611**, 159 (2016), and references therein.
- [24] See e.g. for a non exhaustive list: S. Kanemura, H. Yokoya and Y.-J. Zheng, Nucl. Phys. B **898**, 286 (2015); N. Craig, J. Hajer, Y.-Y. Li, T. Liu and H. Zhang, JHEP **1701**, 018 (2017); W.-S. Hou, M. Kohda and T. Modak, Phys. Lett. B **798**, 134953 (2019).
- [25] D. Eriksson, J. Rathsmann and O. Stål, Comput. Phys. Commun. **181**, 189 (2010).
- [26] M.E. Peskin and T. Takeuchi, Phys. Rev. D **46**, 381 (1992).
- [27] C.D. Froggatt, R.G. Moorhouse and I.G. Knowles, Phys. Rev. D **45**, 2471 (1992).
- [28] H.E. Haber and O. Stål, Eur. Phys. J. C **75**, 491 (2015).
- [29] M. Baak *et al.* [Gfitter Group], Eur. Phys. J. C **74**, 3046 (2014); The latest value of T parameter is obtained from Gfitter website: http://project-gfitter.web.cern.ch/project-gfitter/Oblique_Parameters/
- [30] W.-S. Hou, M. Kohda and T. Modak, Phys. Rev. D **99**, 055046 (2019).
- [31] W.-S. Hou and T. Modak, Phys. Rev. D **101** (2020), 035007.
- [32] M. Ciuchini, G. Degrandi, P. Gambino and G.F. Giudice, Nucl. Phys. B **527**, 21 (1998).
- [33] K.G. Chetyrkin, M. Misiak and M. Munz, Phys. Lett. B **400**, 206 (1997)
- [34] B. Altunkaynak, W.-S. Hou, C. Kao, M. Kohda and B. McCoy, Phys. Lett. B **751**, 135 (2015)
- [35] Y. Amhis *et al.* [HFLAV Collaboration], Eur. Phys. J. C **77**, 895 (2017).
- [36] M. Czakon, P. Fiedler, T. Huber, M. Misiak, T. Schutzmeier and M. Steinhauser, JHEP **1504**,

- 168 (2015).
- [37] A. Crivellin, A. Kokulu and C. Greub, Phys. Rev. D **87**, 094031 (2013).
 - [38] C.-Q. Geng and J.-N. Ng, Phys. Rev. D **38**, 2857 (1988).
 - [39] M. Bona *et al.* [UTfit Collaboration], Phys. Rev. Lett. **97**, 151803 (2006). The New Physics Fit results of 2018 Summer can be found at: <http://www.utfit.org/UTfit/ResultsSummer2018NP>
 - [40] A. L. Kagan and M. Neubert, Phys. Rev. D **58**, 094012 (1998).
 - [41] M. Benzke, S.J. Lee, M. Neubert and G. Paz, Phys. Rev. Lett. **106**, 141801 (2011).
 - [42] S. Watanuki *et al.* [Belle Collaboration], Phys. Rev. D **99**, 032012 (2019).
 - [43] K. Fuyuto, M. Ramsey-Musolf and T. Shen, Phys. Lett. B **788**, 52 (2019).
 - [44] T. Abe, J. Hisano, T. Kitahara and K. Tobioka, JHEP **1401**, 106 (2014) Erratum: [JHEP **1604**, 161 (2016)].
 - [45] D. Bowser-Chao, D. Chang and W. Y. Keung, Phys. Rev. Lett. **79**, 1988 (1997).
M. Kobayashi and T. Maskawa, Prog. Theor. Phys. **49**, 652 (1973).
 - [46] W. Dekens, J. de Vries, M. Jung and K. K. Vos, JHEP **1901**, 069 (2019).
 - [47] C. Abel *et al.* [nEDM], Phys. Rev. Lett. **124** (2020) no.8, 081803.
 - [48] B. Graner, Y. Chen, E. Lindahl and B. Heckel, Phys. Rev. Lett. **116** (2016) no.16, 161601.
 - [49] J. Hisano, D. Kobayashi, W. Kuramoto and T. Kuwahara, JHEP **11** (2015), 085.
 - [50] J. R. Ellis, J. S. Lee and A. Pilaftsis, JHEP **10** (2008), 049.
 - [51] J. Ellis, J. S. Lee and A. Pilaftsis, JHEP **02** (2011), 045;
 - [52] K. Cheung, J. S. Lee, E. Senaha and P. Y. Tseng, JHEP **06** (2014), 149.
 - [53] S. Hacmerolu and Y. K. Semertzidis, Phys. Rev. Accel. Beams **22** (2019) no.3, 034001.
 - [54] V. Anastassopoulos, et al., Rev. Sci. Instrum. **87** (2016) no.11, 115116.
 - [55] A.M. Sirunyan *et al.* [CMS Collaboration], JHEP **1808**, 113 (2018).
 - [56] The ATLAS collaboration [ATLAS Collaboration], ATLAS-CONF-2019-010.
 - [57] M. Aaboud *et al.* [ATLAS Collaboration], JHEP **1811**, 085 (2018).
 - [58] A.M. Sirunyan *et al.* [CMS Collaboration], arXiv:1908.09206 [hep-ex].
 - [59] A.M. Sirunyan *et al.* [CMS Collaboration], arXiv:2001.07763 [hep-ex].
 - [60] To obtain the 95% CL $\sigma(pp \rightarrow bA/H + X) \cdot \mathcal{B}(A/H \rightarrow b\bar{b})$ upper limit for the three benchmark points BPI, BPII and BPIII, we digitized the figure of Ref. [55]. The figure is available in <http://cms-results.web.cern.ch/cms-results/public-results/publications/>

- HIG-16-018/ along with other auxiliary materials (A similar digitization strategy was followed in Ref. [85]).
- [61] J. Alwall *et al.*, JHEP **1407**, 079 (2014).
 - [62] R.D. Ball *et al.* [NNPDF Collaboration], Nucl. Phys. B **877**, 290 (2013).
 - [63] A. Alloul *et al.*, Comput. Phys. Commun. **185**, 2250 (2014).
 - [64] A. M. Sirunyan *et al.* [CMS Collaboration], Eur. Phys. J. C **80**, 75 (2020).
 - [65] T. Sjöstrand, S. Mrenna and P. Skands, JHEP **0605**, 026 (2006).
 - [66] J. de Favereau *et al.* [DELPHES 3 Collaboration], JHEP **1402**, 057 (2014).
 - [67] M.L. Mangano, M. Moretti, F. Piccinini and M. Treccani, JHEP **0701**, 013 (2007).
 - [68] J. Alwall *et al.*, Eur. Phys. J. C **53**, 473 (2008).
 - [69] ATLAS-CMS recommended $t\bar{t}$ cross section predictions: <https://twiki.cern.ch/twiki/bin/view/LHCPhysics/TtbarNNLO>.
 - [70] ATLAS-CMS recommended predictions for single-top cross sections using the Hathor v2.1 program <https://twiki.cern.ch/twiki/bin/view/LHCPhysics/SingleTopRefXsec>.
 - [71] N. Kidonakis, Phys. Rev. D **82**, 054018 (2010).
 - [72] SM Higgs production cross sections at $\sqrt{s} = 14$ TeV: <https://twiki.cern.ch/twiki/bin/view/LHCPhysics/CERNYellowReportPageAt14TeV2010>.
 - [73] J. Campbell, R.K. Ellis and R. Röntsch, Phys. Rev. D **87**, 114006 (2013).
 - [74] Y. Li and F. Petriello, Phys. Rev. D **86**, 094034 (2012).
 - [75] W.-S. Hou, M. Kohda and T. Modak, Phys. Rev. D **96**, 015037 (2017).
 - [76] J.M. Campbell and R.K. Ellis, JHEP **1207**, 052 (2012).
 - [77] G. Cowan, K. Cranmer, E. Gross and O. Vitells, Eur. Phys. J. C **71**, 1554 (2011).
 - [78] W.-S. Hou, M. Kohda, T. Modak, Phys. Lett. B **786**, 212 (2018).
 - [79] W.-S. Hou, G.-L. Lin, C.-Y. Ma, C.-P. Yuan, Phys. Lett. B **409**, 344 (1997).
 - [80] S. Iguro, K. Tobe, Nucl. Phys. B **925**, 560 (2017).
 - [81] Without detailed studies, the process was also discussed by W. Altmannshofer *et al.*, Phys. Rev. D **94**, 115032 (2016); W. Altmannshofer, B. Maddock and D. Tuckler, *ibid.* D **100**, 015003 (2019); and Ref. [80]. See also S. Gori, C. Grojean, A. Juste and A. Paul, JHEP **1801**, 108 (2018), where the $pp \rightarrow t\bar{c}H$ process was discussed.
 - [82] W.-S. Hou, M. Kohda and T. Modak, Phys. Rev. D **98**, 075007 (2018).
 - [83] E. Kou *et al.* [Belle-II], PTEP **2019**, 123C01 (2019).

- [84] C.-H. Chen and T. Nomura, Phys. Rev. D **98**, 095007 (2018).
- [85] W.-S. Hou, M. Kohda and T. Modak, Phys. Rev. D **98**, 015002 (2018).
- [86] J. M. Campbell, R. K. Ellis, F. Maltoni and S. Willenbrock, Phys. Rev. D **67**, 095002 (2003).
- [87] D. Dicus, T. Stelzer, Z. Sullivan and S. Willenbrock, Phys. Rev. D **59**, 094016 (1999).
- [88] F. Maltoni, T. McElmurry and S. Willenbrock, Phys. Rev. D **72**, 074024 (2005).
- [89] R. V. Harlander and W. B. Kilgore, Phys. Rev. D **68**, 013001 (2003).
- [90] F. Maltoni, Z. Sullivan and S. Willenbrock, Phys. Rev. D **67**, 093005 (2003).
- [91] J. Pumplin, D. R. Stump, J. Huston, H. L. Lai, P. M. Nadolsky and W. K. Tung, JHEP **0207**, 012 (2002).
- [92] F. Maltoni, G. Ridolfi and M. Ubiali, JHEP **1207**, 022 (2012).
- [93] J. Butterworth *et al.*, J. Phys. G **43**, 023001 (2016).